



This is a repository copy of *Loss of Tribbles pseudokinase-3 promotes Akt-driven tumorigenesis via FOXO inactivation.*

White Rose Research Online URL for this paper:
<http://eprints.whiterose.ac.uk/86508/>

Version: Accepted Version

Article:

Salazar, M., Salazar, M., Salazar, M. et al. (32 more authors) (2015) Loss of Tribbles pseudokinase-3 promotes Akt-driven tumorigenesis via FOXO inactivation. *Cell Death and Differentiation*, 22 (1). 131 - 144. ISSN 1350-9047

<https://doi.org/10.1038/cdd.2014.133>

Reuse

Unless indicated otherwise, fulltext items are protected by copyright with all rights reserved. The copyright exception in section 29 of the Copyright, Designs and Patents Act 1988 allows the making of a single copy solely for the purpose of non-commercial research or private study within the limits of fair dealing. The publisher or other rights-holder may allow further reproduction and re-use of this version - refer to the White Rose Research Online record for this item. Where records identify the publisher as the copyright holder, users can verify any specific terms of use on the publisher's website.

Takedown

If you consider content in White Rose Research Online to be in breach of UK law, please notify us by emailing eprints@whiterose.ac.uk including the URL of the record and the reason for the withdrawal request.



eprints@whiterose.ac.uk
<https://eprints.whiterose.ac.uk/>

**LOSS OF TRIBBLES PSEUDOKINASE-3 PROMOTES AKT-DRIVEN
TUMORIGENESIS VIA FOXO INACTIVATION**

María Salazar^{1,2,#,§}, Mar Lorente^{1,2,#}, Elena García-Taboada¹, Eduardo Pérez Gómez^{1,3},
David Dávila^{1,2}, Patricia Zúñiga-García⁴, Juana María Flores⁵, Antonio Rodríguez⁵,
Zoltan Hegedus⁶, David Mosén-Ansorena⁴, Ana M. Aransay⁷, Sonia Hernández-
Tiedra^{1,2}, Israel López-Valero^{1,2}, Miguel Quintanilla⁸, Cristina Sánchez^{1,3}, Juan L.
Iovanna⁹, Nelson Duseti⁹, Manuel Guzmán^{1,10}, Sheila E. Francis¹¹, Arkaitz
Carracedo^{4,12}, Endre Kiss-Toth¹¹ and Guillermo Velasco^{1,2,*}

¹Department of Biochemistry and Molecular Biology I, School of Biology,
Complutense University, 28040 Madrid, Spain

²Instituto de Investigaciones Sanitarias San Carlos (IdISSC), 28040 Madrid, Spain

³Instituto de Investigación Hospital 12 de Octubre (I+12), 28041 Madrid Spain

⁴CIC bioGUNE, Bizkaia Technology Park, 48160 Derio, Spain

⁵Department of Animal Surgery and Medicine, School of Veterinary, Complutense
University, 28040 Madrid, Spain

⁶Institute of Biophysics, Hungarian Academy of Sciences, H-6726 Szeged, Hungary

⁷CIC bioGUNE-CIBERehd, Bizkaia Technology Park, Derio, Spain

⁸Instituto de Investigaciones Biomédicas Alberto Sols, Consejo Superior de
Investigaciones Científicas-Universidad Autónoma de Madrid (CSIC-UAM), 28029
Madrid, Spain.

⁹Centre de Recherche en Carcérologie de Marseille (CRCM), INSERM UMR 1068,
CNRS UMR 7258, Aix Marseille Université and Institut Paoli Calmette, Marseille,
France

¹⁰Centro de Investigación Biomédica en Red sobre Enfermedades Neurodegenerativas (CIBERNED) and Instituto Ramón y Cajal de Investigaciones Sanitarias (IRYCIS), 28034 Madrid, Spain

¹¹Department of Cardiovascular Science, University of Sheffield, Sheffield S10 2RX, UK

¹²Ikerbasque, Basque Foundation for Science, 48011 Bilbao, Spain

Contact information:

*Corresponding author: Guillermo Velasco, Department of Biochemistry and Molecular Biology I, School of Biology, Complutense University Calle José Antonio Nováis 2, 28040-Madrid, Spain. Phone: +34913944668, Fax: +34913944672; E-mail: gvd@bbml.ucm.es

[#]These authors equally contributed to this work

[§]Current address, Cell Division and Cancer Group, Spanish National Cancer Research Centre (CNIO), Madrid E-28029, Spain

Running title: Trib3 loss enhances tumorigenesis via AKT and FOXO

ABSTRACT

Tribbles pseudokinase 3 (TRIB3) has been proposed to act as an inhibitor of AKT although the precise molecular bases of this activity and whether loss of TRIB3 contributes to cancer initiation and progression remain to be clarified. In this study, by using a wide array of *in vitro* and *in vivo* approaches, including a *Trib3* knock-out mouse, we demonstrate that TRIB3 plays a tumor-suppressing role. We also find that the mechanism by which TRIB3 loss enhances tumorigenesis relies on the dysregulation of the phosphorylation of AKT by the mTORC2 complex, which leads to an enhanced phosphorylation of AKT on Ser473 and the subsequent hyperphosphorylation and inactivation of the transcription factor FOXO3. These observations support the notion that loss of TRIB3 is associated with a more aggressive phenotype in various types of tumors by enhancing the activity of the mTORC2/AKT/FOXO axis.

Keywords: AKT pathway; cancer; cell signalling; pseudokinases.

INTRODUCTION

Pseudokinases constitute a group of proteins that have a kinase-like domain that lacks at least one of the conserved catalytic residues (1, 2). Different studies have shown that some pseudokinases can exhibit low levels of kinase activity, while others play critical roles as activators of their specific targets (1, 2). Moreover, aberrant regulation of pseudokinases has been implicated in the etiology and progression of a variety of diseases, including cancer (3).

The Tribbles family of pseudokinases was first described in *Drosophila* as a negative regulator of cell division in early embryogenesis (4-7). There are three mammalian Tribbles isoforms (Trib1, Trib2 and Trib3), homologues to the *Drosophila* tribbles proteins, and they all share a highly conserved central kinase-like domain, which lacks catalytic residues, and a “tribbles specific” C-terminal domain, which has been proposed to participate in the binding to different Tribbles partners (8).

Tribbles pseudokinase-3 (TRIB3; also named TRB3, NIPK and SKIP3) has been proposed to interact with several proteins, including the transcription factors ATF4 and CHOP (9) as well as with several MAPKs (10). TRIB3 has also been shown to interact and inhibit AKT (11), which has been suggested to suppress insulin signaling (11, 12). In addition, administration of different anticancer agents promotes cancer cell death via TRIB3 up-regulation and the subsequent inhibition of Akt (13-19). However, the precise molecular bases of the regulation of Akt by TRIB3 and whether loss of this pseudokinase may contribute to cancer initiation and progression remains to be clarified.

In this study we investigated the effect of the genetic inactivation of TRIB3 in several cellular and animal models of cancer. Our findings indicate that genetic inhibition of TRIB3 enhances tumorigenesis and that this effect is due - at least

primarily - to a selective inactivation of the transcription factor FOXO by the mTORC2/AKT axis.

RESULTS

Genetic inhibition of TRIB3 facilitates oncogene transformation and enhances the tumorigenicity of cancer cells

As a first approach to analyze the role of TRIB3 in cancer generation and progression, we investigated the susceptibility to transformation of mouse embryonic fibroblasts (MEFs) derived from *Trib3*^{-/-} and wild type (WT) animals (see Experimental Procedures section and Supplementary Figure S1a-e). Expression of Ras^{V12} (a constitutively active form of the oncogene Ras) was capable of transforming MEFs derived from Trib3 deficient mice (Figure 1a). Similar results were obtained when the SV40 T-large antigen was used (Supplementary Figure S1f), suggesting that loss of TRIB3 facilitates oncogene-induced transformation overall. In line with this idea, a higher number of Trib3-deficient Ras^{V12}-transformed (Figure 1b) and SV40-T large antigen-transformed (Supplementary Figure S1g) MEFs were obtained after several days in culture when compared with their corresponding WT counterparts.

Next, we generated Ras^{V12}/E1A-transformed MEFs as a cellular model to conduct additional mechanistic studies on the role of TRIB3 in cancer. In line with the aforementioned results, a higher percentage of Ras^{V12}/E1A-transformed Trib3-deficient MEFs were positive for Ki67, a marker expressed specifically in dividing cells, when compared with their corresponding WT counterparts (Figure 1c). Likewise, Ras^{V12}/E1A-transformed Trib3^{-/-} MEFs formed four times the number of colonies in soft agar (Figure 1d) as their corresponding WT MEFs. Moreover, this behavior was abolished by re-expressing an HA-tagged form of TRIB3 in Trib3-deficient cells (Figure 1c and 1d), which strongly supports that the enhanced tumorigenic features of Trib3-deficient cells rely solely on the inactivation of this pseudokinase. Furthermore, the onset of tumor xenografts generated by subcutaneous injection of Trib3-deficient

Ras^{V12}/E1A-transformed MEFs in the flank of nude mice was remarkably accelerated compared to that of tumors generated with their WT counterparts (Figure 1e).

Of note, TRIB3 is focally deleted in tumors of epithelial origin and in breast cancer patients (tumourscape dataset; Supplementary Table SI). In addition, analysis of gene expression profiles of cancer patients from published studies reveals that TRIB3 mRNA levels are down-regulated in different tumor types (Supplementary Table SII and SIII). Therefore, we next investigated the effect of the genetic inhibition of TRIB3 in human cancer cell lines. In line with the results obtained with Trib3-deficient MEFs, knock-down of TRIB3 strongly enhanced the ability to form colonies in soft agar of breast carcinoma (BT474) and hepatocellular carcinoma (HepG2) cells lines (Figure 2a). Moreover, TRIB3 silencing increased the number of BT474 and HepG2 cells obtained after several days in culture (Supplementary Figure S2a-b). Furthermore, stable silencing of TRIB3 both accelerated tumor onset and enhanced the rate of tumor growth of xenografts generated with BT474 cells (Figure 2b), and accelerated the onset of HepG2 cell-generated tumors (Figure 2c). Taken together, these observations strongly support that loss of TRIB3 enhances the tumorigenic capacity of different types of cancer cells.

Genetic deletion of Trib3 accelerates the progression of mouse skin papillomas to a more aggressive phenotype

As a first approach to investigate the role of TRIB3 in the control of cancer progression, we analyzed the expression of this pseudokinase in several mouse skin carcinoma cell lines exhibiting different degrees of differentiation and aggressiveness. Specifically, we studied the expression of Trib3 in the MSC11B9/MS11A5 and CarC-R/CarC cell lines, as they constitute homogenous cellular systems of malignant progression

[MSC11B9 and MSC11A5 cells were derived, respectively, from the squamous component and the more undifferentiated region of the same carcinoma (20); and CarC-R is a minority population of less aggressive epithelial cells isolated from the fusocellular carcinoma cell line CarC (21).] Trib3 expression was much lower in MSC11A5 and CarC cells than in their corresponding more differentiated counterparts (Figure 3a). Likewise, Trib3 levels were lower in the spindle cell carcinoma cell line CarB when compared with those of PDV cells (derived from a squamous cell carcinoma cell line) (Figure 3a). Moreover, comparison of Trib3 mRNA levels of normal skin, papillomas and skin carcinomas from mice revealed that Trib3 expression correlated inversely with the aggressiveness of the lesion (Figure 3b). These observations support that down-regulation of Trib3 expression is associated with a more aggressive phenotype in mouse epithelial skin carcinomas.

Based on these observations, we therefore next investigated the effect of Trib3 genetic inactivation on the progression of the lesions observed in mice subjected to the two-stage skin carcinogenesis model as this is one of the best established paradigms for studying the mechanisms underlying malignant transformation *in vivo* (22). Skin tumors were induced in *Trib3^{+/+}* and *Trib3^{-/-}* mice of a mixed C57BL6/J 129/Ola background (see Experimental procedures for details) by topical treatment with a single dose of 7,12-dimethylbenz[a]anthracene (DMBA) followed by a repeated administration of the phorbol ester 12-*O*-tetradecanoylphorbol-13-acetate (TPA) for 20 weeks. After DMBA/TPA challenge, we observed no differences between *Trib3^{+/+}* and *Trib3^{-/-}* mice either in the latency (time from treatment initiation to tumor development) or the size (data not shown) of the skin lesions. However, the frequency of malignant conversion, as determined by the percentage of papillomas that progressed into a more aggressive phenotype [squamous papillomas or squamous papillomas with dysplasia] was

significantly higher in *Trib3*^{-/-} mice than in their corresponding WT littermates after 20 or 32 weeks of the initiation of the treatment (Figure 3c and 3d). Statistically significant differences were not found between *Trib3*^{+/+} and *Trib3*^{-/-} mice in the frequency of “in situ” or squamous cell carcinomas (Supplementary Figure S3).

Loss of TRIB3 enhances the phosphorylation of AKT in cancer cells via mTORC2

TRIB3 has been shown to interact with and inhibit AKT, and dysregulation of this kinase plays a crucial role in cancer generation and progression (23). Therefore, we next investigated whether the enhanced tumorigenic properties of cells in which TRIB3 has been genetically inhibited rely on an enhanced stimulation of the AKT signalling pathway. In line with this idea, Ras^{V12}/E1A-transformed *Trib3*-deficient MEFs, as well as breast carcinoma (BT474) and hepatocellular carcinoma (HepG2) cell lines in which TRIB3 had been knocked-down, exhibited an enhanced phosphorylation of AKT (Figure 4a and Supplementary Figure S4a). Moreover, the increase triggered by the genetic inhibition of *Trib3* in the number of HepG2 and BT474 cells observed after several days in culture was prevented by the pharmacological inhibition of the Akt pathway (Supplementary Figure S4b-c). Likewise, knock-down of TRIB3 enhanced AKT phosphorylation in BT474-, HepG2- and U87MG-cell derived tumor xenografts (Figure 4b). Moreover, tumors derived from Ras^{V12}/E1A-transformed *Trib3*^{-/-} cells exhibited higher phosphorylation levels of AKT than those derived from their corresponding WT counterparts (Figure 4b). Furthermore, cutaneous squamous papillomas from *Trib3*^{-/-} mice also showed higher AKT phosphorylation levels than the papillomas derived from their WT littermates (Figure 4c).

To investigate the mechanism by which the loss of TRIB3 enhances AKT phosphorylation we analyzed the effect of re-expressing an HA-tagged form of TRIB3

in TRIB3-deficient cells. TRIB3 re-expression abolished the enhanced phosphorylation of AKT in Ser 473 but did not modify the phosphorylation of the kinase in Thr 308 (Figure 4d). Since AKT is phosphorylated on Ser473 by the mammalian target of rapamycin complex 2 (mTORC2) (24), we next investigated whether the enhanced phosphorylation of AKT on Ser 473 observed in Trib3-deficient cells relied on the dysregulation of the phosphorylation of AKT by mTORC2. In line with this idea, silencing of the mTORC2 protein component RICTOR or incubation with the mTOR kinase inhibitor torin-1 abolished the enhanced phosphorylation of AKT observed in Ras^{V12}/E1A-transformed *Trib3*^{-/-} MEFs (Figure 4e) as it also did the re-expression of HA-TRIB3 (Supplementary Figure S4d). Moreover, Rictor knock-down prevented the increase (triggered by the genetic inhibition of Trib3) in the number (Figure 4f) and clonogenicity (Figure 4g) of Ras^{V12}/E1A-transformed MEFs, thus suggesting that the tumorigenic properties of Trib3-deficient cells rely on the enhanced phosphorylation of AKT by mTORC2.

Loss of Trib3 enhances the incidence of premalignant and malignant lesions in *Pten*^{+/-} mice

To investigate the relevance of the TRIB3-dependent regulation of AKT in cancer we next analyzed the *in vivo* effect of the genetic inactivation of Trib3 together with that of the tumor suppressor gene phosphatase and tensin homolog (PTEN). PTEN is a highly mutated and frequently lost tumor suppressor in cancer, that negatively regulates the activation of the PI3K pathway through the dephosphorylation of phosphatidylinositol 3,4,5 trisphosphate (PIP₃) (25). Importantly, studies in mice have demonstrated that PTEN is a haplo-insufficient tumor suppressor, as genetic deletion of one copy of the gene is sufficient to unleash oncogenic responses in different organs (26). Accordingly,

Pten^{+/-} mice exhibit an enhanced activation of the AKT pathway and spontaneously develop malignant lesions in different tissues, including prostate, adrenal glands and thyroid (27). Therefore, we crossed *Trib3*^{-/-} mice with *Pten*^{+/-} mice to study whether loss of Trib3 results in an acceleration of these lesions. Eight-month-old animals were sacrificed and histopathological analyses were performed to analyze the presence of pre-malignant and malignant lesions in different tissues. *Trib3*^{-/-} mice exhibited a very low frequency of lesions in the different tissues analyzed. However, *Pten*^{+/-} *Trib3*^{+/-} and *Pten*^{+/-} *Trib3*^{-/-} mice showed a higher frequency of pre-malignant and malignant lesions than *Pten*^{+/-} mice in prostate, adrenal glands and thyroid (Table I, Figure 5a and Supplementary Figure S5). Specifically, 100% of *Pten*^{+/-} *Trib3*^{-/-} vs. 50% of *Pten*^{+/-} mice developed prostatic intraepithelial neoplasia (PIN). Likewise, 67% of *Pten*^{+/-} *Trib3*^{-/-} vs. 37% of *Pten*^{+/-} mice showed hyperplasia of the adrenal glands, and 11% of *Pten*^{+/-} *Trib3*^{-/-} vs. 0% of *Pten*^{+/-} mice developed pheochromocytomas (Figure 5a). Moreover, AKT phosphorylation was increased in hyperplastic adrenal medullas of *Trib3*^{-/-} *Pten*^{+/-} animals when compared with the same lesion in *Pten*^{+/-} mice (Figure 5b). These findings strongly support that loss of Trib3 accelerates the formation of premalignant and malignant lesions in *Pten*^{+/-} mice.

Loss of Trib3 promotes FOXO inactivation

Next, we investigated the targets of AKT that are involved in the enhanced tumorigenic features of cells in which TRIB3 has been genetically inhibited. Remarkably, genetic inhibition of Trib3 led to an enhanced phosphorylation of some of the downstream targets of AKT - namely the transcription factor Forkhead box O3 (FOXO3) and the BH3-only protein BCL2-associated agonist of cell death (BAD) - but not of others such as glycogen synthase kinase 3 (GSK3), or proline rich AKT substrate (PRAS40) (Figure

6a and Supplementary Figure S6a). Likewise, phosphorylation of FOXO3 (but not of the ribosomal protein S6 - whose phosphorylation correlates under many cellular settings with activation of the mTORC1 complex) was enhanced in TRIB3-silenced BT474 and HepG2, cells (Supplementary Figure S6b).

We therefore next investigated whether the enhanced phosphorylation of FOXO3 and BAD observed in TRIB3-deficient cells relied on the dysregulation of the phosphorylation of AKT by mTORC2. In line with this idea, silencing of the mTORC2 protein component Rictor or incubation with the mTOR kinase inhibitor torin-1 abolished the enhanced phosphorylation of FOXO and BAD observed in Trib3-deficient MEFs at the same extent as the re-expression of HA-TRIB3. By contrast, phosphorylation of Pras40 was not modified in any of those experimental conditions (Figure 6b and Supplementary Figure S6c and S6d).

It has been widely reported that the FOXO family of transcription factors plays an important tumor-suppressing role (28). Since genetic inhibition of Trib3 enhances FOXO3 phosphorylation - an event that typically leads to the inactivation and the subsequent sequestration in the cytosol of this transcription factor (23), (29, 30)- we asked whether the activity of FOXO is altered in *Trib3*^{-/-} cells. In line with this idea, FOXO3 exhibited a primarily cytosolic localization in Ras^{V12}/E1A-transformed *Trib3*^{-/-} MEFs subjected to serum withdrawal - an insult that typically leads to FOXO3 translocation to the nucleus (30) (Figure 6c). In contrast, the distribution of FOXO3 was mainly nuclear in Ras^{V12}/E1A-transformed *Trib3*^{+/+} MEFs upon the same experimental conditions (Figure 6c). Likewise, serum withdrawal – which triggers the up-regulation of the Bcl-2 family gene Bcl-2 interacting mediator of cell death (BIM) in a FOXO-dependent manner – led to the activation of the *Bim* promoter in *Trib3*^{+/+} but not in *Trib3*^{-/-} cells (Supplementary Figure S6e). Furthermore, TRIB3 re-expression restored

the ability of serum deprivation to activate the *Bim* promoter in *Trib3*^{-/-} cells, and this effect was abolished when the FOXO binding sites were mutated in this promoter, thus supporting that TRIB3 participates in the regulation of FOXO activity (Figure 6d). To investigate the *in vivo* relevance of our findings we next analyzed whether genetic inhibition of TRIB3 affects the phosphorylation of FOXO in tumor samples. Knock-down of TRIB3 enhanced FOXO3 phosphorylation in HepG2- and BT474- cell derived tumor xenografts (Figure 6e) which occurred in concert with an enhanced expression of the cell proliferation marker Ki67 in those tumors (Supplementary Figure S6f, and S6g). Likewise, tumors derived from Ras^{V12}/E1A-transformed *Trib3*^{-/-} cells exhibited a higher phosphorylation of FOXO (Figure 6e) which was associated with an enhanced Ki67 immunostaining (Supplementary Figure S6h) compared to tumors derived from their corresponding WT counterparts. Furthermore, cutaneous squamous papillomas from *Trib3*^{-/-} mice also showed higher FOXO1/3 phosphorylation levels than the papillomas derived from their WT littermates (Figure 6f).

Loss of Trib3 enhances tumor growth via FOXO inactivation

To study whether the enhanced tumorigenic properties of *Trib3*^{-/-} cells relies on FOXO inhibition, we made use of a construct encoding a form of FOXO3 in which the residues phosphorylated by AKT are mutated to Ala (FOXO-A3). Unlike the endogenous form of FOXO3, the FOXO-A3 mutant localizes in the nucleus of *Trib3*^{-/-} cells (Figure 7a). Moreover, expression of FOXO-A3 in *Trib3*^{-/-} cells re-established the pattern of FOXO-regulated genes (Supplementary Figure S7a), as well as the ability of serum deprivation to activate the *Bim* promoter (Supplementary Figure S7b). In addition, FOXO-A3 expression abolished the increase in the number of cells and the enhanced clonogenicity characteristic of *Trib3*^{-/-} cells (Figure 7b and 7c).

Therefore, we next analyzed the effect of the stable expression of the FOXO-A3 mutant on the ability of Ras^{V12}/E1A-transformed *Trib3*^{-/-} MEFs to generate tumor xenografts. As shown in Figure 7d, the growth rate of tumors generated with Foxo-A3-*Trib3*^{-/-} cells was strongly reduced in comparison with that of *Trib3*^{-/-} cells. Likewise, tumors derived from FOXO-A3-*Trib3*^{-/-} cells exhibited a decreased expression of Ki67 when compared to those generated with *Trib3*^{-/-} cells (Figure 7e). Taken together, these observations strongly support that the enhanced tumorigenic properties of Trib3-deficient cells rely - at least in major part - on the enhanced phosphorylation and subsequent inhibition of FOXO transcription factors.

DISCUSSION

Several observations presented in this work show that TRIB3 plays a remarkable tumor suppressive role. For example, (i) oncogenic transformation is facilitated in MEFs derived from Trib3-deficient mice; (ii) genetic inhibition of TRIB3 enhances proliferation, clonogenicity and the ability to generate tumor xenografts of oncogene-transformed MEFs and of several human cancer cell lines; (iii) loss of TRIB3 enhances the frequency of malignant conversion of papillomas generated in mice subjected to DMBA/TPA treatment; and (iv) loss of TRIB3 enhances the incidence of premalignant and malignant lesions in *Pten*^{+/-} mice.

Our findings demonstrate that the tumor inhibitory role of TRIB3 relies to a large extent on the ability of this pseudokinase to regulate the activity of the AKT pathway. In line with this idea, we found that the genetic inactivation of Trib3 enhances the effect of the deletion of one of the two copies of *Pten* on the formation of pre-malignant and malignant lesions in mice. Of note, AKT phosphorylation is increased in hyperplastic adrenal medullas of *Pten*^{+/-} *Trib3*^{-/-} animals when compared with the same lesion in *Pten*^{+/-} mice, thus suggesting that loss of Trib3 produces an increase in the phosphorylation of AKT that contributes to the malignant progression in this tissue. In the same line of reasoning, *Trib3*^{-/-} mice subjected to the two-step skin carcinogenesis protocol generated papillomas of a more aggressive phenotype and with higher levels of AKT phosphorylation than papillomas generated in WT littermates. Likewise, tumor xenografts generated with Ras^{V12}/E1A-transformed *Trib3*^{-/-} MEFs or with different cancer cell lines in which TRIB3 had been knocked-down exhibited an enhanced phosphorylation of AKT when compared to their corresponding WT or control siRNA-transfected counterparts. Taken together, these observations strongly suggest that

TRIB3 limits the capacity of AKT to become over-activated in response to oncogenic signals.

Our findings also define the mechanism of the tumor suppressive activity of TRIB3 downstream of AKT, which relies on the selective regulation of FOXO3 activity. Thus, re-expression of a mutant form of FOXO3 in which the residues phosphorylated by AKT have been mutated to Ala abolished the enhanced proliferation and clonogenicity of TRIB3-deficient cells and re-established the pattern of FOXO-regulated genes characteristic of WT cells. Furthermore, re-expression of this construct decreased proliferation and growth rate of tumors generated with Trib3-deficient cells. Although care should be taken in the interpretation of data derived from the overexpression of a transcription factor these observations support that FOXO3 inactivation plays a crucial role in the enhanced tumorigenic features of cells in which Trib3 is genetically inactivated. Nevertheless, expression of the FOXO-A3 mutant affected the rate of tumor growth but did not modify the time to occurrence of tumors derived from *Trib3*^{-/-} cells, thereby suggesting that - together with the regulation of FOXO activity – TRIB3 may use additional mechanisms to control tumorigenesis. Further research should therefore clarify the role played by FOXO in the regulation of cell survival and proliferation in cells in which TRIB3 has been genetically inhibited. Likewise, future studies should investigate whether the regulation of additional AKT targets (such as BAD) or of other targets of TRIB3 [including for example those previously implicated in the control of cell proliferation such as ATF-4, SMAD3 or CtIP (3, 31-33)] may also contribute to the tumor-suppressor activity of TRIB3.

TRIB3 has been previously shown to interact with AKT (11, 15), although the precise mechanism by which this interaction regulates the activity of the kinase as well as the physiological consequences of this inhibition had not been completely clarified

yet. Data presented here show that TRIB3 regulates the phosphorylation of AKT by the mTORC2 complex. Of potential relevance in this context, Sabatini's group has shown that genetic ablation of the mTORC2 component RICTOR affects the phosphorylation of FOXO but not of GSK3 or TSC2 (34), thereby suggesting that phosphorylation of AKT in Ser 473 could be sufficient for the kinase to phosphorylate some of its substrates. In line with this observation and with the notion that TRIB3 participates in the regulation of AKT phosphorylation by mTORC2, we found that genetic inactivation of TRIB3 leads to an enhanced phosphorylation of FOXO and BAD, but not of GSK3 or PRAS 40. Moreover, we recently found that treatment with Δ^9 -tetrahydrocannabinol [a compound derived from the plant *Cannabis sativa* that exerts anti-tumor effects in mouse models of cancer (14, 15, 35)] triggers AKT inhibition via an enhanced interaction of TRIB3 with AKT and a subsequent decrease in the interaction of AKT and TRIB3 with the mTORC2 complex (19). Our data also show that Trib3 interacts more strongly with WT AKT, or with AKT mutants in which Thr 308 and Ser 473 have been mutated to Ala, than with AKT mutants in which these two phosphorylatable residues have been mutated to Asp to mimic the negative charge associated with their phosphorylation (author's unpublished observations). Altogether, these observations cogently support that the interaction with TRIB3 negatively regulates AKT by restricting the access of the kinase to the mTORC2 complex (a schematic of the proposed model is shown in Figure 7f). Moreover, our findings also show that TRIB3 may contribute to the regulation of AKT selectivity for some of its substrates. Of note, total Akt levels are increased in Trib3^{-/-} RasV12/E1A-transformed MEFs when compared with their corresponding WT counterparts. Although this effect is much less pronounced than that of TRIB3 genetic inactivation on Akt phosphorylation and does not take place in HepG2 or BT474 cells in which TRIB3 expression was silenced, these

observations suggest that TRIB3 may also play a role on the regulation of AKT stability.

Analysis of gene expression profiles of cancer patients from published studies reveals that TRIB3 mRNA levels are down-regulated in different tumor types (Supplementary Table II and III). Likewise, high TRIB3 protein levels are associated with good prognosis in breast cancer patients (36). In addition, TRIB3 is focally deleted in tumors of epithelial origin (tumourscape dataset; Supplementary Table I), thus supporting that loss or down-regulation of TRIB3 is an event associated with human cancer. Nevertheless, other studies have found an up-regulation of TRIB3 mRNA levels in human cancers (33, 37). In addition, previous observations by other laboratories indicate that TRIB3 can enhance proliferation and invasiveness of cancer cells *in vitro* (31-33), and a recent study has shown that knock-down of TRIB3 produces a moderate increase in the growth of orthotopic xenografts generated with MDA-231 breast cancer cells (38). A plausible explanation for the apparently contradictory results obtained here and in those studies could be the existence of differences in the genetic alterations, the degree of differentiation or other relevant phenotypic characteristics in the cell lines used in the various studies. In support of this idea, and as shown in the present study, silencing of TRIB3 produces heterogeneous effects on the tumorigenic properties of different cancer cell lines as it enhances the rate growth of tumors generated with U87MG cells (data not shown), accelerates the onset of HepG2 cell-derived tumors, and hastens both processes in tumors generated with BT474 cells. Thus, although the findings presented here cogently support that genetic inhibition of TRIB3 enhances tumorigenesis in several genetic contexts and, specifically, in the presence of activating mutations of *Ras* or the deletion of one of the copies of *Pten*, further research should clarify whether inactivation or enhanced expression of TRIB3 may produce a different

outcome in a distinct genetic or cellular context. It is worth noting that it has been reported that TRIB3 null animals show up-regulation of TRIB1 and TRIB2 in at least some tissues (39). Since TRIB2 is associated with induction of acute myelogenous leukemia (AML) (40, 41) and TRIB1 with other malignancies (42, 43), changes in the levels of the other Tribbles isoforms may also contribute to the phenotype observed in Trib3^{-/-} animals.

In summary, results presented here show that genetic inhibition of TRIB3 increases tumorigenesis in several animal models of cancer and that this effect is due – at least primarily – to the enhanced phosphorylation of AKT by the mTORC2 complex and the subsequent hyperphosphorylation and inactivation of FOXO3. These results may help to set the basis for the development of novel targeted therapies for the management of cancer.

MATERIALS AND METHODS

A list of the reagents used, primer sequences, antibodies and other materials, together with additional details of all techniques used in this study can be found in Supplemental Experimental Procedures.

Generation of Trib3^{-/-} mice

Trib3^{+/-} mice [B6;129S5-Trib3Gt(OST324148)Lex/Ieg obtained from European Mouse Mutant Archive, EMMA; ID: EM-02346, LEXKO-1947] were back crossed with C57/BL6 for ten generations and were then inter-crossed to generate homozygous knockout embryos. This line was developed using the OST324148 OmniBank® ES cell line from a sequence tagged gene trap library (44). Briefly, the gene trap vector included a two expression cassettes (Supplementary Figure S1a). The first cassette encoded for a splice acceptor site (SA), followed by a fusion protein of beta-galactosidase and neomycin, thereby disrupting transcription of the targeted mRNA. The second cassette encoded for a “diagnostic marker”, followed by a splice donor site and was used to determine the site of insertion for the targeting vector by 3’ RACE. Using this gene trap vector, the TRIB3 allele was targeted in the first intron. (Supplementary Figure S1b). The sequence shown in Supplementary Figure S1C includes 250 nucleotides on either side of the insertion site, denoted by an asterisk (data kindly provided by Lexicon Pharmaceuticals). Exons 2-4 encode for the TRIB3 Open Reading Frame (highlighted in red). Insertion of the gene trap vector prevented the expression of the TRIB3 protein, as demonstrated by an anti TRIB3 western blot (Supplementary Figure S1e) and did not produce a truncated version of Trib3 as we had previously proposed in a previous work (19).

Generation of Pten^{+/-} Trib3^{-/-} animals

Pten^{+/-} mice (C57/Bl6/J) were kindly provided by Dr Manuel Serrano (Spanish Cancer Research Center, Madrid, Spain). Characterization of these animals has been previously described (45). *Pten*^{+/-} mice were crossed with *Trib3*^{+/-} mice and the progeny intercrossed. Animals of the different genotypes were sacrificed at 8 months of age and histopathological analyses of different organs were performed. All procedures involving animals were performed with the approval of the Complutense University Animal Experimentation Committee in compliance with Spanish and European official regulations

Genotyping

Tail genomic DNA were isolated using standard procedures. Primers used for PCR genotyping were: 5' CCGCGACGAATGAAAGGTTTA 3'; 5' AGACTCCGAGAGCTGCTCAGTTAGG 3' for wt (*Trib3*) allele (483 bp) and 5' CCGCGACGAATGAAAGGTTTA 3', 5' AAATGGCGTTACTTAAGCTAGCTTGC3' for KO (*Trib3*) allele (381 bp). PCR conditions were 40 cycles (30 s at 95 °C, 30 s at 65 °C and 30 s at 72 °C; supplementary Figure S1). Genotyping of *Pten* animals has been previously described (45).

Skin Chemical Carcinogenesis model: animals and treatments

As pure C57BL6/J mice are refractory to DMBA/ TPA-induced carcinogenesis, *Trib3*^{+/-} animals were bred to the DMBA/TPA-sensitive 129/Ola strain. Heterozygous animals from this progeny were inter-crossed to generate the *Trib3*^{+/+} and *Trib3*^{-/-} littermates used in this study (129/SvEvBrd_C57BL6/J mixed genetic background). For the two-stage carcinogenesis experiments, tumors were induced on the shaved dorsal skin of WT (n=15) and TRB3 KO (n= 20) mice by topical application of a single dose of DMBA (32 mg in 200 ml of acetone), followed by twice-weekly applications of TPA

(12.5 mg in 200 ml of acetone) for 20 weeks. The number of tumors (42 mm in diameter) was recorded weekly. TPA treatment was ended after 20 weeks, and animals were left untreated until week 32 after DMBA initiation to allow the development of carcinomas. Tumors were collected at different time points and histologically typed as previously described. At the end of the experiments, mice were killed and tumors or skin were collected. Samples were divided into portions that were (1) frozen in Tissue-Tek (Sakura Finetek Europe, Zoeterwoude, The Netherlands) for immunofluorescence staining, (2) snap-frozen for protein and RNA extraction or (3) fixed in 10% buffered formalin, pH 7.2, for 24-72 hours. All tissues were processed by standard histologic techniques for the production of 4 μ m thick sections stained with hematoxylin and eosin. Skin slides were studied and classified according to the International Classification of Rodent Tumours (1993). In four cases of animal death, necropsies were performed on all mice within 24 hours of death and samples of cutaneous masses, lung, liver, kidney, spleen, stomach, small and large intestine, adrenal and thyroid gland, reproductive tract and brain were collected and processed the same way.

Cell culture

U87MG (human glioma cell line), BT474 (human breast cancer cells) and HEPG2 cells (human hepatocellular carcinoma cell line) were obtained from the American Culture Collection (Rockville, MD). CarC, CarCR, MSC11B9, MSC11A5, PDV and CarB murine skin carcinoma cell lines (see text and Supplementary Experimental procedures for further details) were obtained from Miguel Quintanilla. [CarC-R is a less aggressive epithelial cell line isolated from the fusocellular carcinoma cell line CarC (21); MSC11B9 (B9) and MSC11A5 (A5) cells were derived, respectively, from the squamous component and the more undifferentiated region of the same carcinoma (20);

PDV cells were derived from a squamous cell carcinoma and CarB cells from a spindle cell carcinoma].

Trib3^{+/+} and *Trib3*^{-/-} mouse embryonic fibroblasts (MEFs) were extracted as previously described (46) and transformed using different retroviral vectors to generate RasV¹²-MEFs, RasV12/E1A-MEFs, SV40 T-large antigen-MEF and FOXO3/RasV¹²/E1A/-MEFs. Transformed/stably transfected MEFs correspond to a polyclonal mix of at least 20 different selected clones). Cells were cultured in DMEM containing 10% FBS and penicillin/ streptomycin (5µg/ml). When required, cells were seeded at a density of 5 000-10 000 cells/cm² and transferred to medium containing 0.5% FBS (except RasV12/E1A-transformed MEFs, that were transferred to media containing 2% FBS) 18 h before performing the different treatments.

Genetic knock-down by small interfering RNA

SMARTpool siRNA duplexes (a combination of four siRNAs into a single pool, which guarantees an efficiency of silencing of at least 75%; Dharmacon, Lafayette, CO, US) were used to transiently silence the expression of the indicated genes. Controls were transfected with a non-targeted control siRNA. Transfection efficiency was higher than 70% as monitored with a control fluorescent (red) siRNA (siGLO RISC-Free siRNA, Dharmacon)

Infection with TRB3 shRNA- human lentiviral particles

A pool of concentrated transduction-ready viral particles containing 3 shRNAs target-specific (or 3 shRNA non-targeted control) constructs; Santa Cruz Biotechnology; Heidelberg, Germany) was used to infect human cancer cell lines. Clones of stably-silenced (or control shRNA transduced) cells were selected. At least 20 different

selected clones were pooled for each of the cell lines generated.

Luciferase assays

Cells were transfected with a luciferase reporter constructs containing different promoters along with a Renilla luciferase expression plasmid (pRL-TK) for normalization.

***In vivo* generation of tumor xenografts**

Tumors were induced by subcutaneous injection in nude mice (Harlan Interfauna Iberica, Barcelona, Spain) of 4×10^6 cells in PBS supplemented with 0.1% glucose.

Statistics

Except when otherwise stated, statistical analysis was performed by ANOVA with a post-hoc analysis by the Student-Neuman-Keuls test (paired or unpaired). Differences were considered significant when the P value was less than 0.05. Wilcoxon signed-rank test was used in the analysis of cumulative number of papillomas found in animals subjected to the DMBA/TPA treatment.

ACKNOWLEDGMENTS

This work was supported by grants from Spanish Ministry of Economy and Competitiveness (MINECO) (PS09/01401; PI12/02248, FR2009-0052 and IT2009-0053 to GV), Comunidad de Madrid (S2011/BMD-2308 to MG), Fundación Mutua Madrileña (AP101042012 to GV) and Breast Cancer Campaign (2012NovSP033 to EKT and GV). Purchase of the TRIB3-deficient mice (LEXKO-1947) line was funded

by the Wellcome Trust. MS was recipient of a fellowship from Spanish Ministry of Education and Science (MEC), a research formation contract from Comunidad de Madrid and a Postdoctoral Research Contract from Fundación Científica Asociación Española Contra el Cáncer (AECC); ML was sequentially the recipient of a ‘Juan de la Cierva’ contract, a postdoctoral contract from Spanish Ministry of Education and Science (MEC) and a postdoctoral contract from Comunidad de Madrid. AC is supported by the Ramón y Cajal award (Spanish Ministry of Education), the Basque Department of Industry, Tourism and Trade (Etortek), Marie Curie Reintegration grant (277043), Movember Global Action Plan, ISCIII (PI10/01484) and the Basque Government of health (2012111086) and education (PI2012-03). EPG was the recipient of a Postdoctoral Research Contract from AECC. We would like to thank Dr Dario Alessi (Dundee University, UK) for his expert scientific and technical support and for kindly providing antibodies for the immunoprecipitation experiments. We also would like to thank other members of our laboratories for their continuous support. The authors declare that they do not have any conflict of interest.

Authors’s contributions

MS and ML participated in the design of the study, the performance of in vitro and in vivo experiments, the analysis and interpretation of the data and manuscript writings. EGT performed in vitro and in vivo experiments, EPG participated in the design of skin carcinogenesis experiments, analysis and interpretation of the data and critical reading of the manuscript, DD participated in the design and performance of in vitro experiments, analysis and interpretation of the data and critical reading of the manuscript, PZ participated in the performance of in vitro experiments and analysis of the data, JMF and AR performed anatomo-pathological analyses in mice. ZH, DMA and

AMA performed bio-informatics analyses, SHT and ILV participated in the performance of in vitro experiments, MQ, provided materials and participated in the design of experiments with skin cancer cells, CS, JLI, ND, MG, SEF, AC and EKT participated in the design of the study and critical reading of the manuscript, GV, conceived and coordinated the study and wrote the manuscript.

REFERENCES

1. Boudeau J, Miranda-Saavedra D, Barton GJ, Alessi DR. Emerging roles of pseudokinases. *Trends Cell Biol* 2006 Sep; **16** (9): 443-452.
2. Zeqiraj E, van Aalten DM. Pseudokinases-remnants of evolution or key allosteric regulators? *Curr Opin Struct Biol* 2010 Dec; **20** (6): 772-781.
3. Zhang H, Photiou A, Grothey A, Stebbing J, Giamas G. The role of pseudokinases in cancer. *Cell Signal* 2012 Jun; **24** (6): 1173-1184.
4. Grosshans J, Wieschaus E. A genetic link between morphogenesis and cell division during formation of the ventral furrow in *Drosophila*. *Cell* 2000 May 26; **101** (5): 523-531.
5. Mata J, Curado S, Ephrussi A, Rorth P. Tribbles coordinates mitosis and morphogenesis in *Drosophila* by regulating string/CDC25 proteolysis. *Cell* 2000 May 26; **101** (5): 511-522.
6. Rorth P, Szabo K, Texido G. The level of C/EBP protein is critical for cell migration during *Drosophila* oogenesis and is tightly controlled by regulated degradation. *Mol Cell* 2000 Jul; **6** (1): 23-30.
7. Seher TC, Leptin M. Tribbles, a cell-cycle brake that coordinates proliferation and morphogenesis during *Drosophila* gastrulation. *Curr Biol* 2000 Jun 1; **10** (11): 623-629.
8. Hegedus Z, Czibula A, Kiss-Toth E. Tribbles: a family of kinase-like proteins with potent signalling regulatory function. *Cell Signal* 2007 Feb; **19** (2): 238-250.
9. Ohoka N, Yoshii S, Hattori T, Onozaki K, Hayashi H. TRB3, a novel ER stress-inducible gene, is induced via ATF4-CHOP pathway and is involved in cell death. *EMBO J* 2005 Mar 23; **24** (6): 1243-1255.
10. Kiss-Toth E, Bagstaff SM, Sung HY, Jozsa V, Dempsey C, Caunt JC, *et al.* Human tribbles, a protein family controlling mitogen-activated protein kinase cascades. *J Biol Chem* 2004 Oct 8; **279** (41): 42703-42708.
11. Du K, Herzig S, Kulkarni RN, Montminy M. TRB3: a tribbles homolog that inhibits Akt/PKB activation by insulin in liver. *Science* 2003 Jun 6; **300** (5625): 1574-1577.
12. Koo SH, Satoh H, Herzig S, Lee CH, Hedrick S, Kulkarni R, *et al.* PGC-1 promotes insulin resistance in liver through PPAR-alpha-dependent induction of TRB-3. *Nat Med* 2004 May; **10** (5): 530-534.
13. Carracedo A, Gironella M, Lorente M, Garcia S, Guzman M, Velasco G, *et al.* Cannabinoids induce apoptosis of pancreatic tumor cells via endoplasmic reticulum stress-related genes. *Cancer Res* 2006 Jul 1; **66** (13): 6748-6755.

14. Carracedo A, Lorente M, Egia A, Blazquez C, Garcia S, Giroux V, *et al.* The stress-regulated protein p8 mediates cannabinoid-induced apoptosis of tumor cells. *Cancer Cell* 2006 Apr; **9** (4): 301-312.
15. Salazar M, Carracedo A, Salanueva IJ, Hernandez-Tiedra S, Lorente M, Egia A, *et al.* Cannabinoid action induces autophagy-mediated cell death through stimulation of ER stress in human glioma cells. *The Journal of clinical investigation* 2009 Apr 1; **119** (5): 1359-1372.
16. Nicoletti-Carvalho JE, Nogueira TC, Gorjao R, Bromati CR, Yamanaka TS, Boschero AC, *et al.* UPR-mediated TRIB3 expression correlates with reduced AKT phosphorylation and inability of interleukin 6 to overcome palmitate-induced apoptosis in RINm5F cells. *J Endocrinol* 2010 Aug; **206** (2): 183-193.
17. Vara D, Salazar M, Olea-Herrero N, Guzman M, Velasco G, Diaz-Laviada I. Anti-tumoral action of cannabinoids on hepatocellular carcinoma: role of AMPK-dependent activation of autophagy. *Cell death and differentiation* 2011 Jul; **18** (7): 1099-1111.
18. Zhang J, Wen HJ, Guo ZM, Zeng MS, Li MZ, Jiang YE, *et al.* TRB3 overexpression due to endoplasmic reticulum stress inhibits AKT kinase activation of tongue squamous cell carcinoma. *Oral Oncol* 2011 Oct; **47** (10): 934-939.
19. Salazar M, Lorente M, Garcia-Taboada E, Hernandez-Tiedra S, Davila D, Francis SE, *et al.* The pseudokinase tribbles homologue-3 plays a crucial role in cannabinoid anticancer action. *Biochim Biophys Acta* 2013 Apr 6.
20. Burns PA, Kemp CJ, Gannon JV, Lane DP, Bremner R, Balmain A. Loss of heterozygosity and mutational alterations of the p53 gene in skin tumours of interspecific hybrid mice. *Oncogene* 1991 Dec; **6** (12): 2363-2369.
21. Pons M, Cigudosa JC, Rodriguez-Perales S, Bella JL, Gonzalez C, Gamallo C, *et al.* Chromosomal instability and phenotypic plasticity during the squamous-spindle carcinoma transition: association of a specific T(14;15) with malignant progression. *Oncogene* 2005 Nov 17; **24** (51): 7608-7618.
22. Abel EL, Angel JM, Kiguchi K, DiGiovanni J. Multi-stage chemical carcinogenesis in mouse skin: fundamentals and applications. *Nat Protoc* 2009; **4** (9): 1350-1362.
23. Pearce LR, Komander D, Alessi DR. The nuts and bolts of AGC protein kinases. *Nat Rev Mol Cell Biol* 2009 Jan; **11** (1): 9-22.
24. Zoncu R, Efeyan A, Sabatini DM. mTOR: from growth signal integration to cancer, diabetes and ageing. *Nat Rev Mol Cell Biol* 2010 Jan; **12** (1): 21-35.
25. Salmena L, Carracedo A, Pandolfi PP. Tenets of PTEN tumor suppression. *Cell* 2008 May 2; **133** (3): 403-414.

26. Nardella C, Carracedo A, Salmena L, Pandolfi PP. Faithfull modeling of PTEN loss driven diseases in the mouse. *Curr Top Microbiol Immunol* 2011; **347**: 135-168.
27. Hollander MC, Blumenthal GM, Dennis PA. PTEN loss in the continuum of common cancers, rare syndromes and mouse models. *Nat Rev Cancer* 2011 Apr; **11** (4): 289-301.
28. Dansen TB, Burgering BM. Unravelling the tumor-suppressive functions of FOXO proteins. *Trends Cell Biol* 2008 Sep; **18** (9): 421-429.
29. Biggs WH, 3rd, Meisenhelder J, Hunter T, Cavenee WK, Arden KC. Protein kinase B/Akt-mediated phosphorylation promotes nuclear exclusion of the winged helix transcription factor FKHR1. *Proc Natl Acad Sci U S A* 1999 Jun 22; **96** (13): 7421-7426.
30. Brunet A, Bonni A, Zigmond MJ, Lin MZ, Juo P, Hu LS, *et al.* Akt promotes cell survival by phosphorylating and inhibiting a Forkhead transcription factor. *Cell* 1999 Mar 19; **96** (6): 857-868.
31. Bowers AJ, Scully S, Boylan JF. SKIP3, a novel Drosophila tribbles ortholog, is overexpressed in human tumors and is regulated by hypoxia. *Oncogene* 2003 May 8; **22** (18): 2823-2835.
32. Hua F, Mu R, Liu J, Xue J, Wang Z, Lin H, *et al.* TRB3 interacts with SMAD3 promoting tumor cell migration and invasion. *J Cell Sci* 2011 Oct 1; **124** (Pt 19): 3235-3246.
33. Xu J, Lv S, Qin Y, Shu F, Xu Y, Chen J, *et al.* TRB3 interacts with CtIP and is overexpressed in certain cancers. *Biochim Biophys Acta* 2007 Feb; **1770** (2): 273-278.
34. Guertin DA, Stevens DM, Thoreen CC, Burds AA, Kalaany NY, Moffat J, *et al.* Ablation in mice of the mTORC components raptor, rictor, or mLST8 reveals that mTORC2 is required for signaling to Akt-FOXO and PKCalpha, but not S6K1. *Dev Cell* 2006 Dec; **11** (6): 859-871.
35. Velasco G, Sanchez C, Guzman M. Towards the use of cannabinoids as antitumour agents. *Nat Rev Cancer* 2012 Jun; **12** (6): 436-444.
36. Wennemers M, Bussink J, Grebenchtchikov N, Sweep FC, Span PN. TRIB3 protein denotes a good prognosis in breast cancer patients and is associated with hypoxia sensitivity. *Radiother Oncol* 2011 Oct; **101** (1): 198-202.
37. Wennemers M, Bussink J, Scheijen B, Nagtegaal ID, van Laarhoven HW, Raleigh JA, *et al.* Tribbles homolog 3 denotes a poor prognosis in breast cancer and is involved in hypoxia response. *Breast Cancer Res* 2011; **13** (4): R82.

38. Izrailit J, Berman HK, Datti A, Wrana JL, Reedijk M. High throughput kinase inhibitor screens reveal TRB3 and MAPK-ERK/TGFbeta pathways as fundamental Notch regulators in breast cancer. *Proc Natl Acad Sci U S A* 2013 Jan 29; **110** (5): 1714-1719.
39. Zareen N, Biswas SC, Greene LA. A feed-forward loop involving Trib3, Akt and FoxO mediates death of NGF-deprived neurons. *Cell death and differentiation* 2013 Dec; **20** (12): 1719-1730.
40. Rishi L, Hannon M, Salome M, Hasemann M, Frank AK, Campos J, *et al.* Regulation of Trib2 by an E2F1-C/EBPalpha feedback loop in AML cell proliferation. *Blood* 2014 Apr 10; **123** (15): 2389-2400.
41. Zanella F, Renner O, Garcia B, Callejas S, Dopazo A, Peregrina S, *et al.* Human TRIB2 is a repressor of FOXO that contributes to the malignant phenotype of melanoma cells. *Oncogene* 2010 May 20; **29** (20): 2973-2982.
42. Jin G, Yamazaki Y, Takuwa M, Takahara T, Kaneko K, Kuwata T, *et al.* Trib1 and Evf1 cooperate with Hoxa and Meis1 in myeloid leukemogenesis. *Blood* 2007 May 1; **109** (9): 3998-4005.
43. Mashima T, Soma-Nagae T, Migita T, Kinoshita R, Iwamoto A, Yuasa T, *et al.* TRIB1 supports prostate tumorigenesis and tumor-propagating cell survival by regulation of endoplasmic reticulum chaperone expression. *Cancer Res* 2014 Jun 24.
44. Zambrowicz BP, Abuin A, Ramirez-Solis R, Richter LJ, Piggott J, BeltrandelRio H, *et al.* Wnk1 kinase deficiency lowers blood pressure in mice: a gene-trap screen to identify potential targets for therapeutic intervention. *Proc Natl Acad Sci U S A* 2003 Nov 25; **100** (24): 14109-14114.
45. Di Cristofano A, Pesce B, Cordon-Cardo C, Pandolfi PP. Pten is essential for embryonic development and tumour suppression. *Nat Genet* 1998 Aug; **19** (4): 348-355.
46. Salazar M, Hernandez-Tiedra S, Torres S, Lorente M, Guzman M, Velasco G. Detecting autophagy in response to ER stress signals in cancer. *Methods Enzymol* 2011; **489** (2011): 297-317.

FIGURE LEGENDS

Figure 1. Genetic inhibition of TRIB3 facilitates oncogene transformation and enhances the tumorigenicity of transformed embryonic fibroblasts

(a) Effect of RasV¹² expression on the ability of Trib3^{+/+} and Trib3^{-/-} mouse embryonic fibroblast (MEFs) to form colonies in soft agar (cells were transduced with a retroviral vector encoding Ras^{V12})(mean \pm SD; n=3; ***P* < 0.01 from Trib3^{+/+} MEFs).

(b) Effect of transduction with a retroviral vector encoding Ras^{V12} or with the empty retroviral vector pBABE on Trib3^{+/+} and Trib3^{-/-} MEFs cell number . Data correspond to the number of cells at each time point (as determined by crystal violet staining) relative to the number of cells at day 0 for each experimental condition (mean \pm SD; n=3; ***P* < 0.01 from RasV¹²-Trib3^{+/+} MEFs).

(c) Effect of HA-TRIB3 expression on the percentage of Ki67-positive RasV¹²/E1A-transformed Trib3^{+/+} and Trib3^{-/-} MEFs. Data correspond to the percentage of Ki67-positive cells relative to the total number of cells in each experimental condition (mean \pm SD; n=4; ***P* < 0.01 from empty vector-transfected Trib3^{+/+} cells and ^{##}*P* < 0.01 relative to empty vector-transfected Trib3^{-/-} cells). Upper panel: Western blot analysis of TRIB3 expression. A representative experiment (n=4) is shown.

(d) Effect of HA-TRIB3 expression on the ability RasV¹²/E1A-transformed Trib3^{+/+} and Trib3^{-/-} MEFs to form colonies in soft agar. (mean \pm SD; n=6; ***P* < 0.01 relative to empty vector-transfected Trib3^{+/+} cells and [#]*P* < 0.05 relative to empty vector-transfected Trib3^{-/-} cells).

(e) Effect of Trib3 genetic inactivation on the growth of tumor xenografts generated by subcutaneous injection of RasV¹²/E1A-transformed MEFs in nude mice. Data correspond to the mean volume change \pm SEM at each time point (n=8 for each condition; 4 x 10⁶ cells were injected in each experimental condition). Right panel: Data correspond to the time elapsed from the injection of the cells until the tumors reach an average volume of 250 \pm 25 mm³ (mean \pm SEM; n=8 for each condition; ***P* < 0.01 from tumors generated with Trib3^{-/-} MEFs).

Figure 2. Genetic inhibition of TRIB3 enhances the tumorigenicity of cancer cell lines

(a) Effect of TRIB3 stable knockdown on the ability of BT474 (left panel) and HepG2 (right panel) cells to form colonies in soft agar. [mean \pm SD; n=3; ***P* < 0.01 relative to

BT474 or HepG2 cells stably transduced with a lentiviral vector encoding a control (non-targeted) shRNA sequence (shC)].

(b-c) Effect of TRIB3 stable knockdown on the growth of tumor xenografts generated by subcutaneous injection of BT474 (b) and HepG2 (c) cells in nude mice. Data on the lower panels correspond to tumor volume [mean \pm SEM; n= 6 for each condition; * P < 0.05 and ** P < 0.01 from tumors generated with shC BT474 (b) and shC HEPG2 (c) cells]. Upper panels: Data correspond to the time elapsed from the injection of the cells until the tumors reach an average volume of 250 ± 25 mm³ (mean \pm SEM; n=6 for each condition).

Insets in panels b and c show the expression of human TRIB3 mRNA levels (hTRIB3) (as determined by RT-PCR) in tumors generated with shC- and shTRIB3-transduced cells.

Figure 3. TRIB3 genetic inactivation accelerates the malignant progression of mouse skin papillomas

(a) TRIB3 mRNA levels as determined by real-time quantitative PCR in different mouse skin cancer cell lines. Data are expressed as the mean fold-increase \pm SD relative to the corresponding less differentiated cell lines (n=3; ** P < 0.01 compared to undifferentiated cells).

(b) TRIB3 mRNA levels as determined by real-time quantitative PCR in samples derived from normal skin, papillomas, squamous cell carcinomas (SCC) grades I and II (SCCI/II) and SCC grades III and IV (SCCIII/IV) obtained from mice subjected to the two-stage model of skin carcinogenesis. Data correspond to TRIB3 mRNA levels and are expressed as the mean fold change \pm SD relative to normal skin (n=8, 8, 6 and 6 for normal skin, papillomas, SCCI/II and SCCIII/IV, respectively; ** P < 0.01 from normal skin; ^{##} P < 0.01 from papillomas and ^{aa} P < 0.01 from SCC I/II samples).

(c) Effect of TRIB3 genetic inactivation on the degree of differentiation and aggressiveness of the skin lesions appeared in *Trib3*^{-/-} and *Trib3*^{+/+} mice subjected to the two-stage skin carcinogenesis protocol. (Animals were sacrificed 20 or 32 weeks after the administration of the DMBA treatment and subsequently subjected to histopathological analyses). Data are expressed as the mean number of squamous papillomas or squamous papillomas with dysplasia per animal \pm SEM. [week 20: 6 *Trib3*^{+/+} and 5 *Trib3*^{-/-} mice; week 32: 7 *Trib3*^{+/+} and 9 *Trib3*^{-/-} mice; ** P < 0.01 or * P < 0.05 from *Trib3*^{+/+} animals].

(d) Representative images of hematoxylin/eosin (upper panel, 2x) and PCNA staining (lower panel, 10x) of squamous papillomas and squamous papillomas with severe dysplasia observed in *Trib3^{+/+}* and *Trib3^{-/-}* mice. See also Supplementary Fig S3.

Figure 4. Loss of TRIB3 enhances the phosphorylation of AKT in cancer cells via mTORC2

(a) Effect of TRIB3 genetic inactivation on AKT phosphorylation of RasV¹²/E1A-transformed MEFs. Values below each of the Western blots correspond to the densitometric analysis of the ratio Phospho-Akt (P-Akt)/tubulin and total Akt (t-Akt)/tubulin respectively and are expressed as the mean fold change \pm s.d. relative to *Trib3^{+/+}* cells. Data on the right panel correspond to the P-Akt/t-Akt ratio and are expressed as the mean fold change \pm s.d. relative to *Trib3^{+/+}* cells. (n=4; ** $P < 0.01$ from *Trib3^{+/+}* cells)

(b) Effect of TRIB3 genetic inactivation (left panel) or stable knockdown (middle and right panel) on AKT phosphorylation as determined by Western blot analysis of tumor xenografts generated by subcutaneous injection of RasV¹²/E1A-transformed MEFs (left panel), HepG2 (middle panel) and BT474 (right panel) cells in nude mice. Data correspond to the densitometric analysis of AKT phosphorylation expressed as the P-Akt/t-Akt ratio relative to *Trib3^{+/+}*-MEFs (left panel), shC BT474 (middle panel) or shC BT474 (right panel) tumors (n=3; mean \pm SD) [$**P < 0.01$ from tumors generated with *Trib3^{+/+}* MEFs, shC HEPG2 or shC BT474 cells].

(c) Effect of TRIB3 genetic inactivation on AKT phosphorylation of cutaneous squamous papillomas. Representative images (40x) of P-AKT and t-AKT immunohistochemistry staining from 3 cutaneous squamous papillomas per experimental condition are shown.

(d) Effect of HA-TRIB3 expression on the phosphorylation of Akt on Thr 308 and Ser 473 of RasV¹²/E1A-transformed *Trib3^{-/-}* MEFs (n=3, a representative experiment is shown). Upper panel: AKT was immunoprecipitated from cell extracts obtained from RasV¹²/E1A-transformed *Trib3^{+/+}* or *Trib3^{-/-}* MEFs transfected with an empty vector (pCDNA) or a plasmid encoding HA-TRIB3. Lower panel: Analysis of total AKT and HA-TRIB3 levels in the corresponding whole cell extracts (samples were loaded by duplicate).

(e) Effect of RICTOR knock-down (left panel) or incubation in the presence of torin1 (250 nM, 18 h; right panel) on the phosphorylation of AKT on Ser 473 of RasV¹²/E1A-transformed *Trib3*^{+/+} or *Trib3*^{-/-} MEFs (n=3; a representative Western blot analysis is shown). Values below each of the Western blots correspond to the P-Akt/t-Akt ratio and are expressed as the mean fold change ± s.d. relative to shC, *Trib3*^{+/+} (left panel) or veh-treated *Trib3*^{+/+} (right panel) cells. [n=3; ** *P* < 0.01 from shC *Trib3*^{+/+} (left panel) or veh-treated shC *Trib3*^{+/+} (right panel) cells and ^{##} *P* < 0.01 from shC *Trib3*^{-/-} cells (left panel) or from veh-treated *Trib3*^{-/-} (right panel) cells]

(f) Effect of RICTOR knock-down on the number (as estimated by the MTT test) of RasV¹²/E1A-transformed *Trib3*^{+/+} and *Trib3*^{-/-} MEFs. Data are expressed as the mean fold increase ± SD relative to siC *Trib3*^{+/+} MEFs at 24 h; (n=4; ***P* < 0.01 from siC-transfected *Trib3*^{+/+} MEFs; ^{##} *P* < 0.01 from siC-transfected *Trib3*^{-/-} MEFs).

(g) Effect of RICTOR knock-down on the ability of RasV¹²/E1A-transformed *Trib3*^{+/+} and *Trib3*^{-/-} MEFs to form colonies in soft agar (n=3. Images of one representative experiment are shown).

(e-g) Transfection with RICTOR siRNA reduced RICTOR mRNA levels (as determined by quantitative real-time PCR) of *Trib3*^{+/+} and *Trib3*^{-/-} cells by 83±1 % and 91±2 % respectively (p < 0.01 from the corresponding siC-transfected RasV12/E1A-MEFs; n=4).

Figure 5. Loss of TRIB3 enhances the incidence of premalignant and malignant lesions in *Pten*^{+/-} mice.

(a) Effect of the genetic inactivation of TRIB3 on the incidence of premalignant and malignant lesions in the adrenal glands of *Pten*^{+/-} mice. Data are expressed as the percentage of animals of each genotype that exhibit hyperplasia of the adrenal glands (upper panel) or pheochromocytomas (middle panels). Bottom panel: Representative microphotographs (10x) of the different lesions observed in the adrenal glands of *Pten*^{+/-} *Trib3*^{+/-} and *Pten*^{+/-} *Trib3*^{-/-} animals stained with hematoxylin/eosin.

(b) Representative microphotographs of anti-phospho AKT and total Akt immunostaining of the adrenal glands of wild type, *Pten*^{+/-} and *Pten*^{+/-} *Trib3*^{-/-} animals. Note that the hyperplastic region located in the medulla of the adrenal gland exhibits strong phospho-AKT immuno-staining in *Pten*^{+/-} *Trib3*^{-/-} mice but not in *Pten*^{+/-} mice

(n=3; 40x). Insets show details of the different panels at higher magnification. See also Supplementary Figure S5.

Figure 6. Loss of TRIB3 promotes FOXO inactivation

(a) Effect of TRIB3 genetic inactivation on the phosphorylation of FOXO, of Ras^{V12}/E1A-transformed MEFs. Values below the Western blots correspond to the densitometric analysis of the ratio Phospho-FOXO (P-FOXO)/tubulin and total FOXO (t-FOXO)/tubulin respectively and are expressed as the mean fold change \pm s.d. relative to *Trib3*^{+/+} cells. Data on the right panel correspond to the P-FOXO/t-FOXO ratio and are expressed as the mean fold change \pm s.d. relative to *Trib3*^{+/+} cells. (n=4; ** $P < 0.01$ from *Trib3*^{+/+} cells)

(b) Effect of TRIB3 re-expression (upper panel), and RICTOR knock-down (lower panel) on the phosphorylation of FOXO, of Ras^{V12}/E1A-transformed *Trib3*^{+/+} and *Trib3*^{-/-} MEFs. Values in the bottom of the panels correspond to the P-FOXO/t-FOXO ratio and are expressed as the mean fold change \pm s.d. relative to pCDNA *Trib3*^{+/+} (upper panel) or siC-transfected *Trib3*^{+/+} (lower panel) MEFs. [n=3; ** $P < 0.01$ and * $P < 0.05$ from pCDNA *Trib3*^{+/+} (upper panel) or siC-transfected *Trib3*^{+/+} (lower panel) cells. Transfection with RICTOR siRNA reduced RICTOR mRNA levels (as determined by quantitative real-time PCR) of *Trib3*^{+/+} and *Trib3*^{-/-} cells by 83 \pm 1 % and 91 \pm 2 % respectively (n=4; $P < 0.01$ from the corresponding siC-transfected RasV12/E1A-MEFs).

(c) Effect of serum withdrawal on the sub-cellular distribution (as determined by cellular fractionation and subsequent Western blot analysis of cytosolic and nuclear fractions) of endogenous FOXO in Ras^{V12}/E1A-transformed *Trib3*^{+/+} and *Trib3*^{-/-} MEFs. β -actin was used as loading control. I κ B- α and Lamin A/B were used as markers of the cytosolic and the nuclear fractions, respectively (n=3; a representative experiment is shown).

(d) Effect of serum withdrawal on the activity of the *Bim* promoter of Ras^{V12}/E1A-transformed *Trib3*^{-/-} MEFs transfected with a vector encoding HA-TRIB3 or a control plasmid and co-transfected with a luciferase reporter vector containing the sequence of the *Bim* promoter (WT or mutated on the FOXO binding sites). Data correspond to the luciferase activity and are expressed as the mean fold increase \pm SD relative to HA-

TRIB3-transfected *Trib3*^{-/-} cells incubated in the presence of serum (n=3; **P* < 0.05 from serum-treated HA-TRIB3-transfected *Trib3*^{-/-} cells).

(e) Effect of TRIB3 genetic inactivation (e, left panel) or stable knockdown (e, middle and right panels) on FOXO phosphorylation as determined by Western blot analysis of tumor xenografts generated by subcutaneous injection of RasV¹²/E1A-transformed MEFs (left panel), HepG2 (middle panel) and BT474 cells (right panel) in nude mice.

Values in the bottom of the panels correspond to the P-FOXO/t-FOXO ratio and are expressed as the mean fold change ± s.d. relative to *Trib3*^{+/+} tumors (left panel) or shC HepG2 tumors (middle panel) or shC BT474 tumors (right panel) [n=3; ** *P* < 0.01 or * *P* < 0.05 from tumors generated with *Trib3*^{+/+} MEFs, shC HEPG2 or shC BT474 cells].

(f) Effect of TRIB3 genetic inactivation on FOXO3 phosphorylation of cutaneous squamous papillomas. Representative images (40x) of phospho-FOXO1/3 or total FOXO3 immunohistochemistry staining from 3 cutaneous squamous papillomas per experimental condition are shown. See also Supplementary Figure S6.

Figure 7. Loss of TRIB3 enhances tumor growth via FOXO inactivation

(a) Upper panel: Analysis of FOXO protein levels in RasV¹²/E1A-transformed *Trib3*^{+/+} and *Trib3*^{-/-} MEFs stably transfected with a constitutively active version of FOXO (FOXOA3) or the corresponding empty vector (pBABE). Lower panel: Sub-cellular distribution (as determined by cellular fractionation and subsequent Western blot analysis of cytosolic and nuclear fractions) of FOXO protein in RasV¹²/E1A-transformed *Trib3*^{-/-} MEFs stably transfected with FOXOA3. β-actin was used as loading control. Iκβ-α and Lamin A/B were used as markers of the cytosolic and the nuclear fractions, respectively (n=3; a representative experiment is shown).

(b) Effect of TRIB3 genetic inactivation and stable expression of FOXOA3 on the number of RasV¹²/E1A-transformed MEFs (as estimated by the MTT test) at the indicated time points. Data are expressed as the mean fold change ± SD relative to pBABE-*Trib3*^{+/+} cells at 24 h (mean ± SD; n=3; ***P* < 0.01 from pBABE-*Trib3*^{+/+} cells; ^{##}*P* < 0.01 from pBABE-*Trib3*^{-/-} cells).

(c) Effect of TRIB3 genetic inactivation and stable expression of FOXOA3 on the ability of RasV¹²/E1A-transformed MEFs to form colonies in soft agar (n=3. A representative experiment is shown).

(d) Effect of FOXOA3 stable expression and TRIB3 genetic inactivation on the growth of tumor xenografts generated by subcutaneous injection of RasV¹²/E1A-transformed

MEFs in nude mice data are expressed as the mean tumour volume \pm SEM for each experimental condition (n=8 for each condition; volume of Trib3^{-/-} FOXOA3 cell-derived tumor is compared with that of tumors derived from Trib3^{-/-} pBabe cells; ***P* < 0.01 from pBABE-Trib3^{-/-} cell-derived tumors). Lower panel: analysis of FOXO protein levels in tumors derived from FOXOA3-Trib3^{-/-} and pBABE-Trib3^{-/-} cells.

(e) Analysis of Ki67 immunostaining in samples from tumors derived from pBABE-Trib3^{+/+}, pBABE-Trib3^{-/-} and FOXOA3-Trib3^{-/-} cells. Values in the lower right corner of microphotographs correspond to the Ki67-stained area relative to the total number of nuclei in each section and are expressed as the mean fold change relative to pBABE-Trib3^{+/+} tumors \pm SD. (***P* < 0.01 from pBABE-Trib3^{+/+} tumors; ##*P* < 0.01 from pBABE-Trib3^{-/-} tumors; 18 sections for each of 3 dissected tumors for each condition were counted). Representative microphotographs are shown.

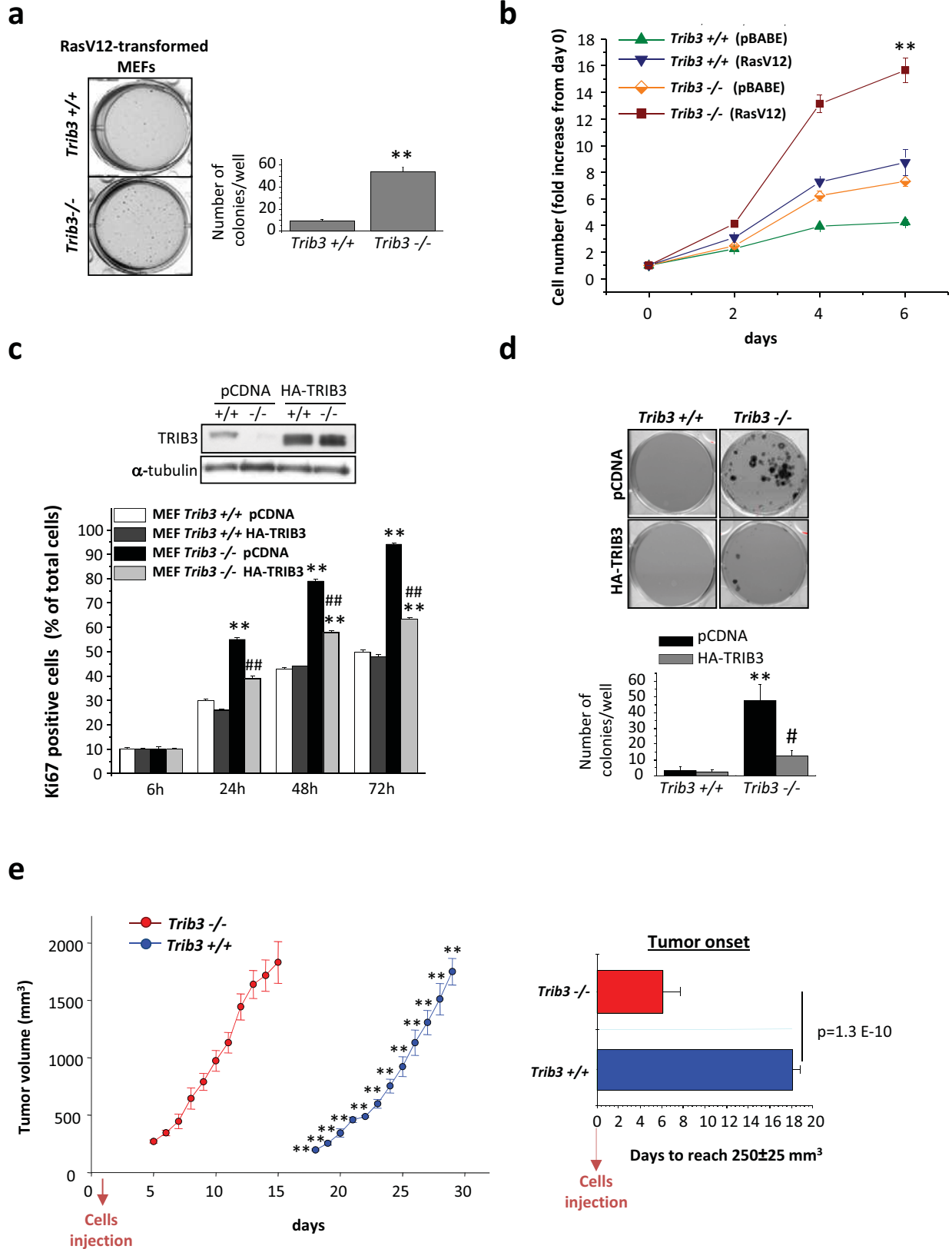
(f) Proposed model of the mechanism by which TRIB3 controls tumorigenesis. TRIB3 interacts with AKT, which regulates the phosphorylation of the kinase by the mTORC2 complex (left panel). Genetic inhibition of TRIB3 in combination with different oncogenic signals facilitates the hyper-phosphorylation of AKT on Ser 473 by the mTORC2 complex and the subsequent hyper-phosphorylation and inactivation of the transcription factor FOXO3 (as well as of the BH3-only protein BAD) but not of other AKT downstream targets. The hyper-phosphorylation and inactivation of FOXO is responsible - at least in part - for the enhanced tumorigenic features of TRIB3-deficient cells. See also Supplementary Figure S7 and Supplementary Table II.

	Wild Type n=14	<i>Trib3</i> +/- n=9	<i>Trib3</i> -/- n=12	<i>Pten</i> +/- n=8	<i>Pten</i> +/- <i>Trib3</i> +/- n=14	<i>Pten</i> +/- <i>Trib3</i> -/- n=9
Lymph node						
Lymphoid hyperplasia submandibular	0 %	0 %	0 %	62 %	57 %	67 %
Lymphoid hyperplasia abdominal ganglia	0 %	0 %	0 %	0 %	0 %	22 %
Thyroid						
Hyperthyroidism	0 %	11 %	0 %	12 %	64 %	55 %
Thyroid adenoma	0 %	0 %	0 %	0 %	14 %	11 %
Liver						
Lymphoid infiltrates	0 %	0 %	8 %	12 %	0 %	0 %
Steatohepatitis	0 %	0 %	0 %	0 %	7 %	11 %
Intestine						
Adenoma	0 %	0 %	0 %	12 %	7 %	11 %
Spleen						
Lymphoid hyperplasia	0 %	0 %	0 %	0 %	0 %	11 %

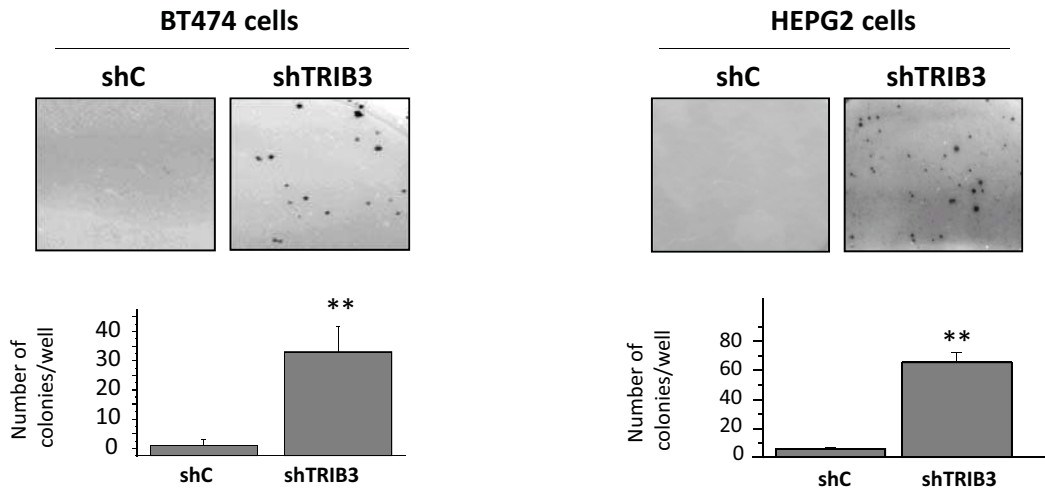
	Wild Type n=9	<i>Trib3</i> +/- n=5	<i>Trib3</i> -/- n=4	<i>Pten</i> +/- n=4	<i>Pten</i> +/- <i>Trib3</i> +/- n=12	<i>Pten</i> +/- <i>Trib3</i> -/- n=3
Anterior Prostate						
Hyperplasia	11 %	0 %	0 %	75 %	100 %	100 %
Adenoma	0 %	0 %	0 %	25 %	36 %	67 %
PIN	0 %	0 %	0 %	50 %	63 %	33 %
Dorsal Prostate						
Hyperplasia	11 %	0 %	0 %	50 %	83 %	100 %
Adenoma	0 %	0 %	0 %	0 %	25 %	0 %
PIN	0 %	0 %	0 %	50 %	75 %	100 %

Table I. Loss of TRIB3 accelerates the formation of premalignant and malignant lesions in *Pten*^{+/-} mice

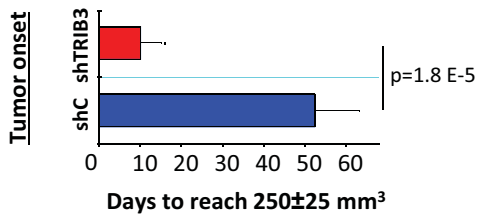
Incidence of pre-malignant and malignant lesions (as determined by histopathological analysis) in different tissues and organs of 8 month-old wild type, *Trib3*^{+/-}, *Trib3*^{-/-}, *Pten*^{+/-}, *Pten*^{+/-} *Trib3*^{+/-} and *Pten*^{+/-} *Trib3*^{-/-} mice.



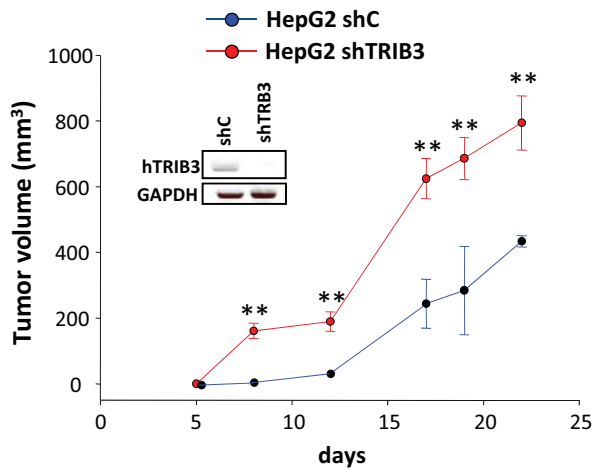
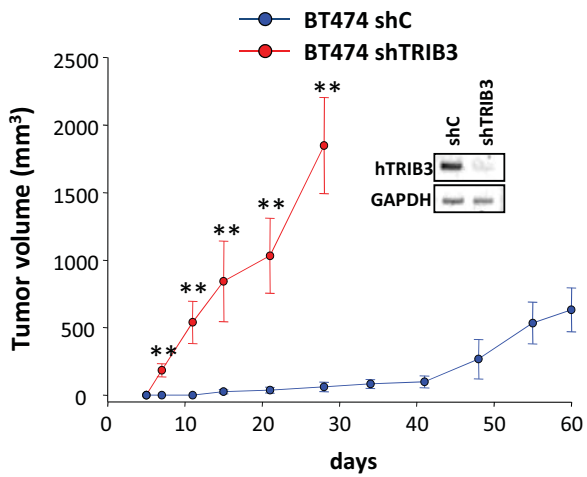
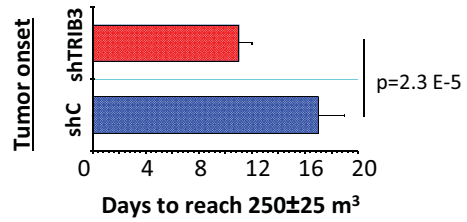
a

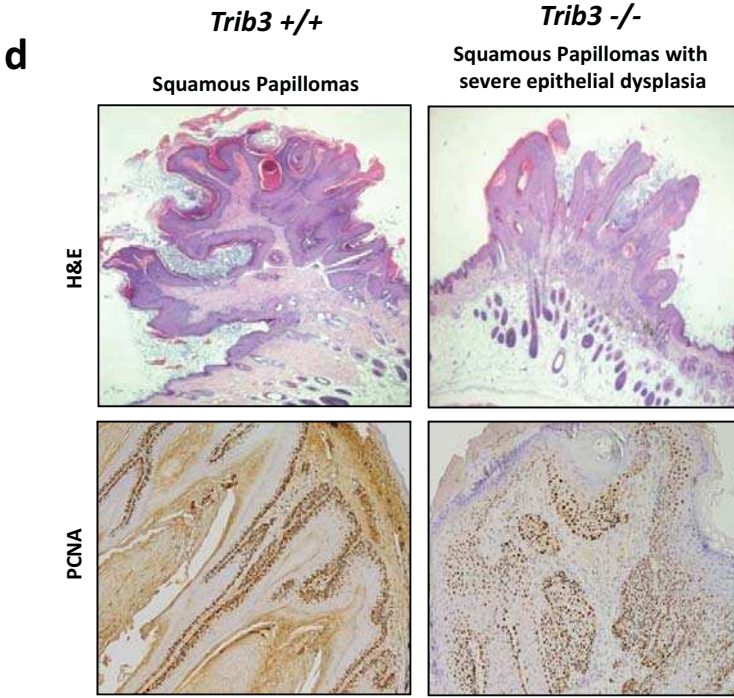
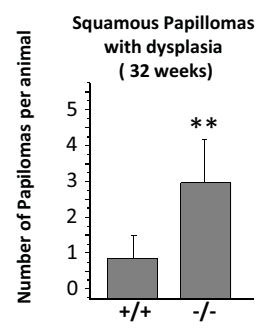
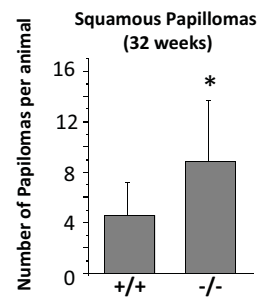
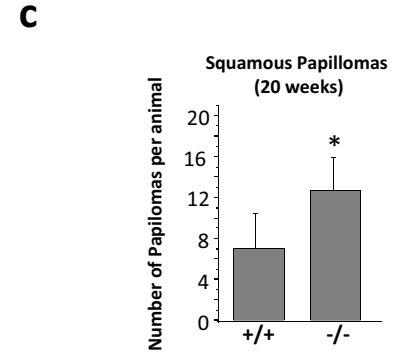
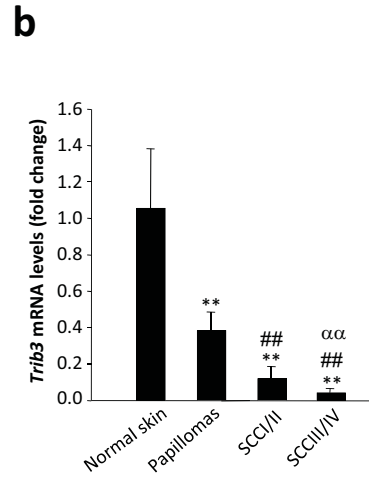
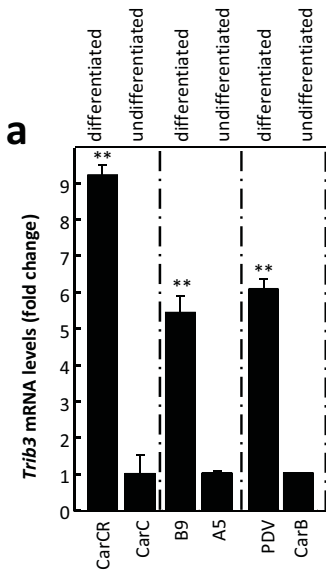


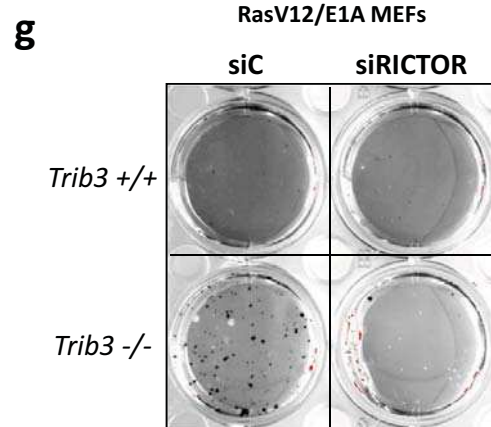
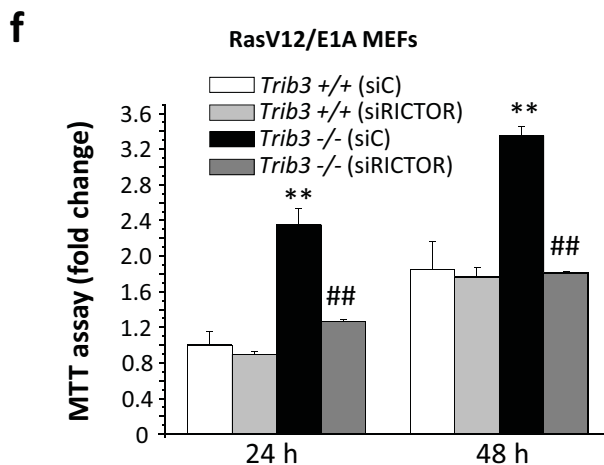
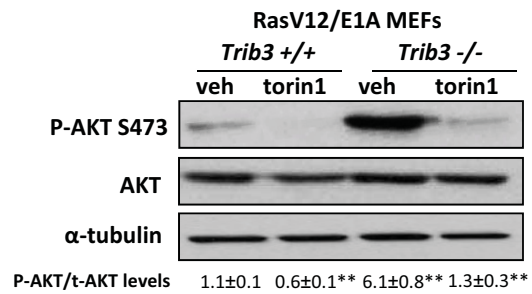
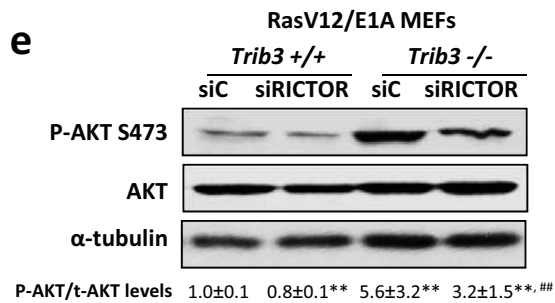
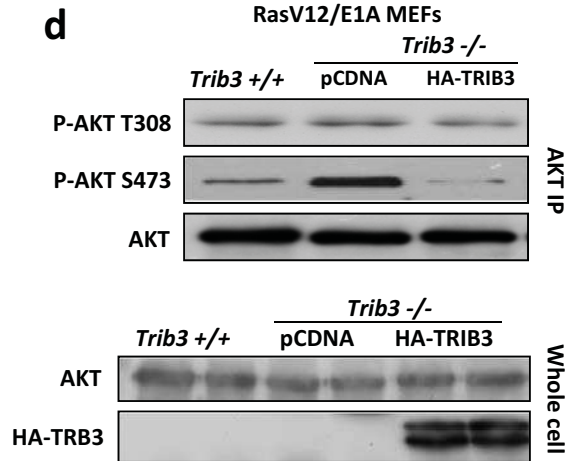
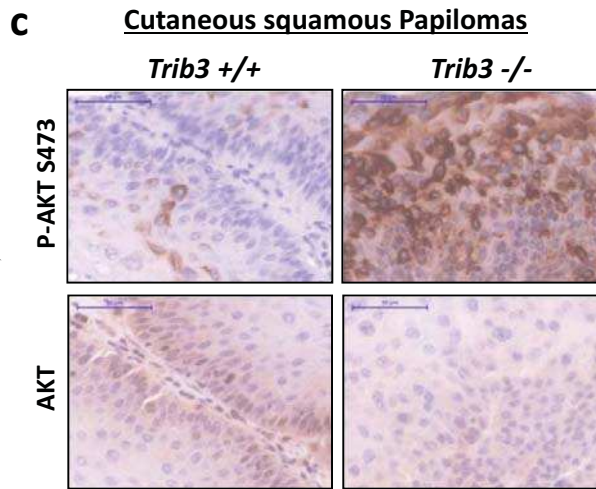
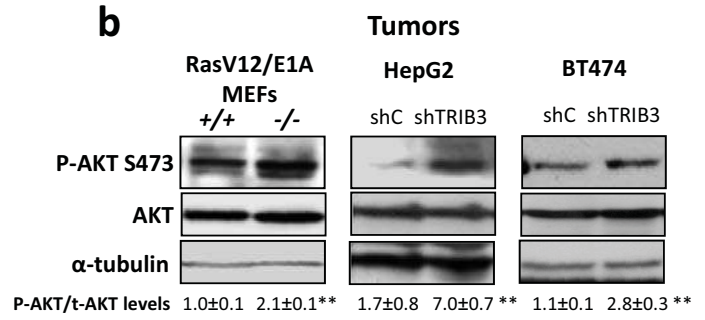
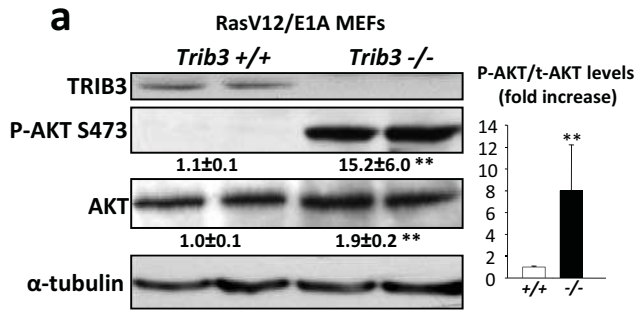
b



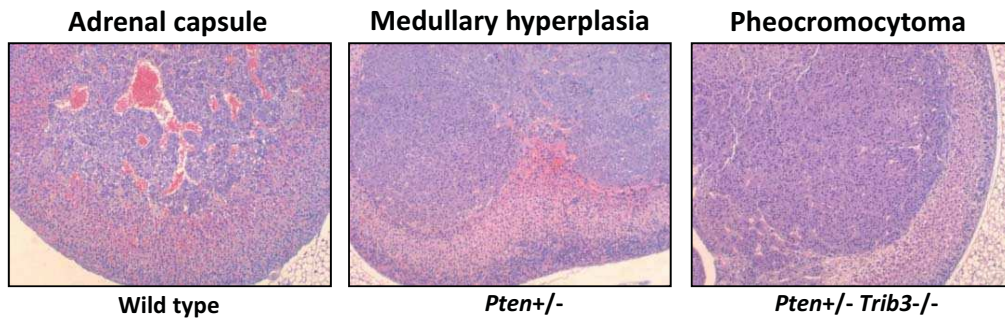
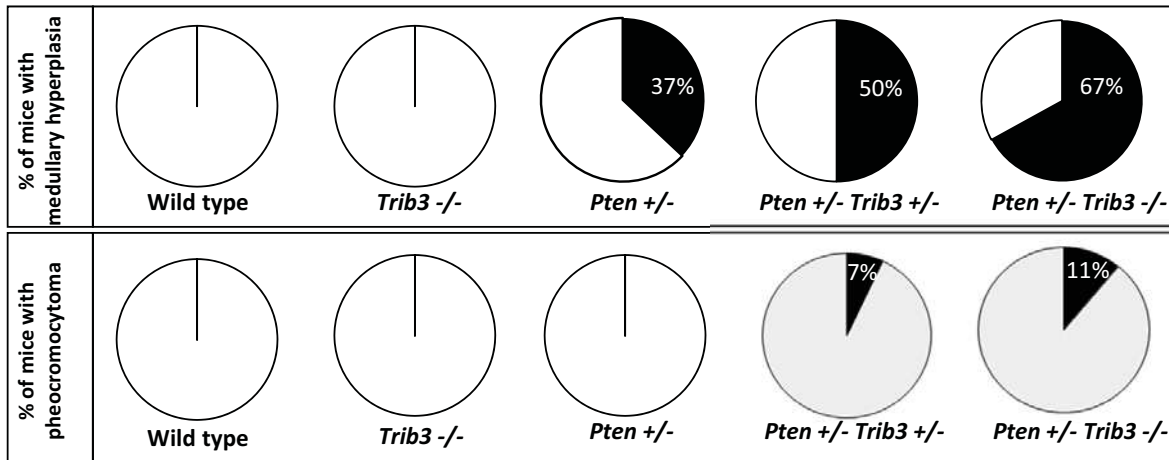
c



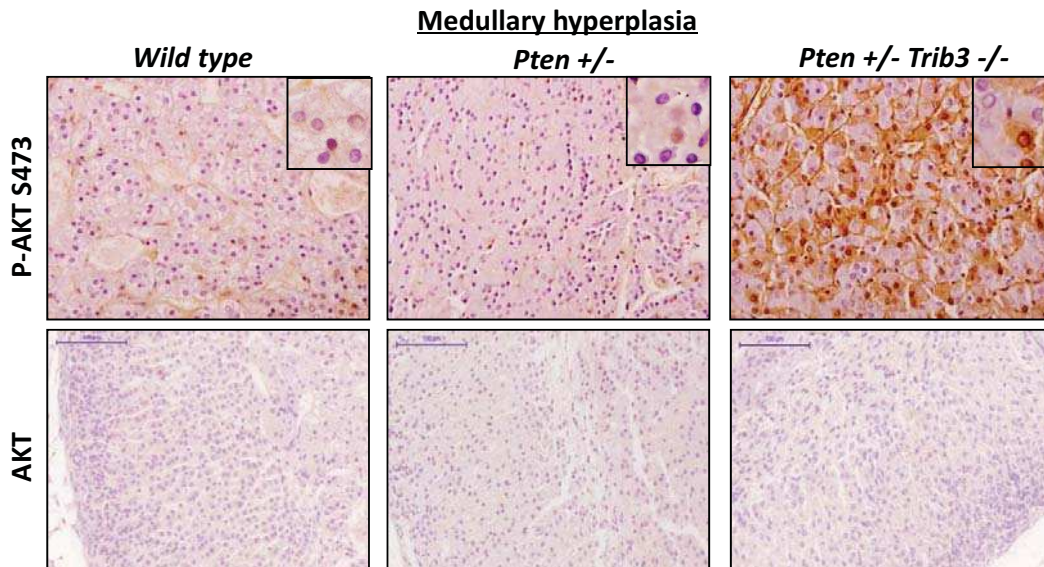


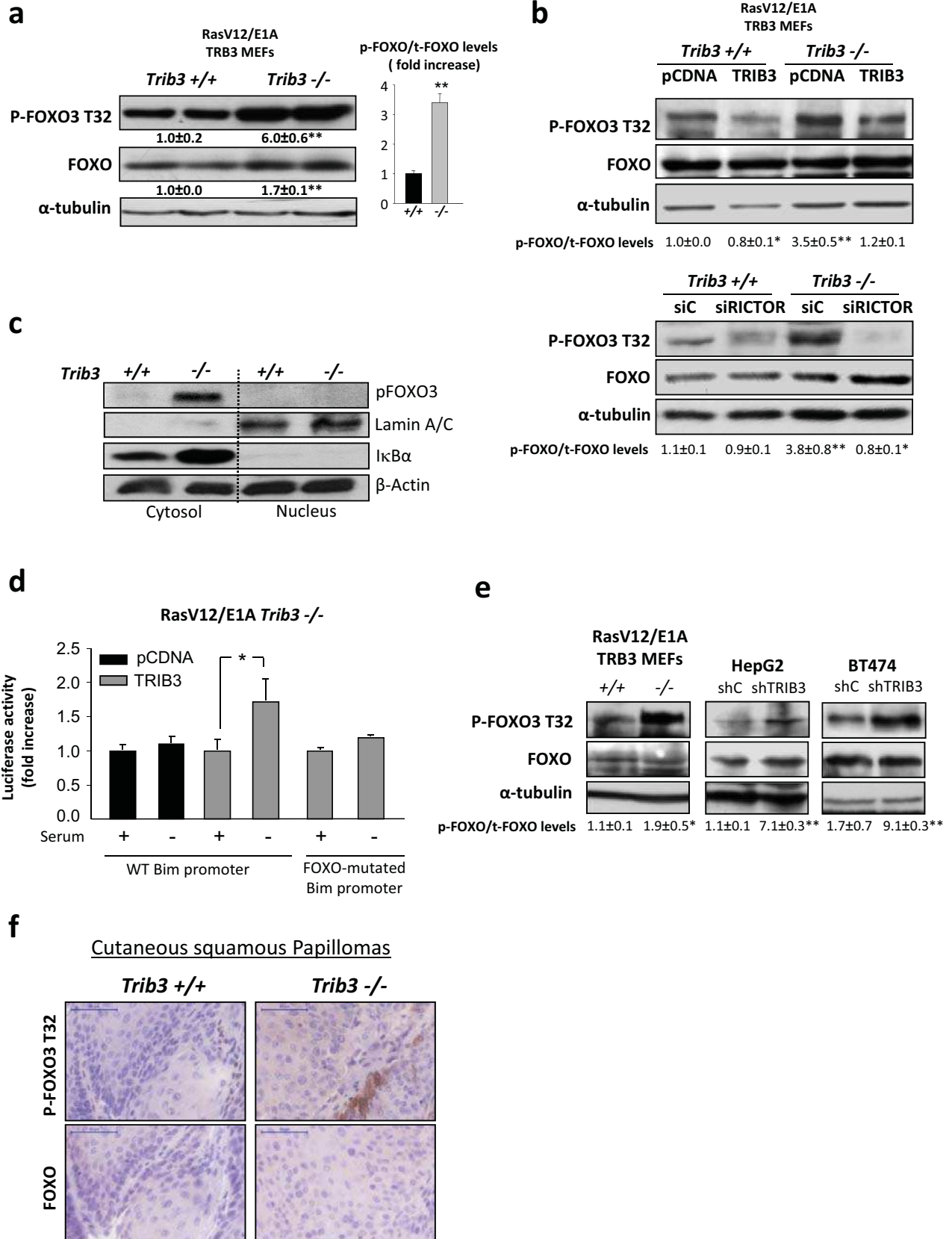


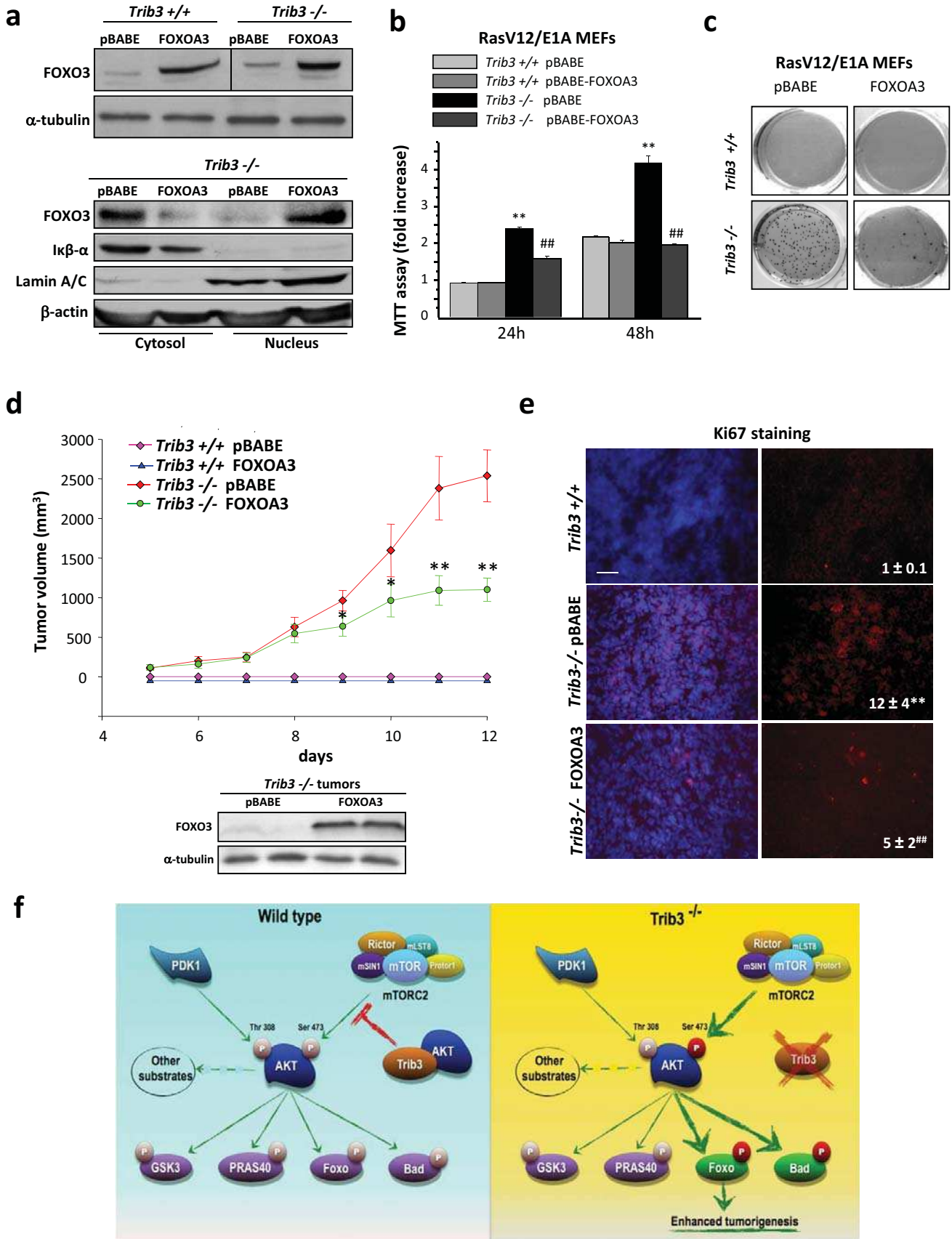
a

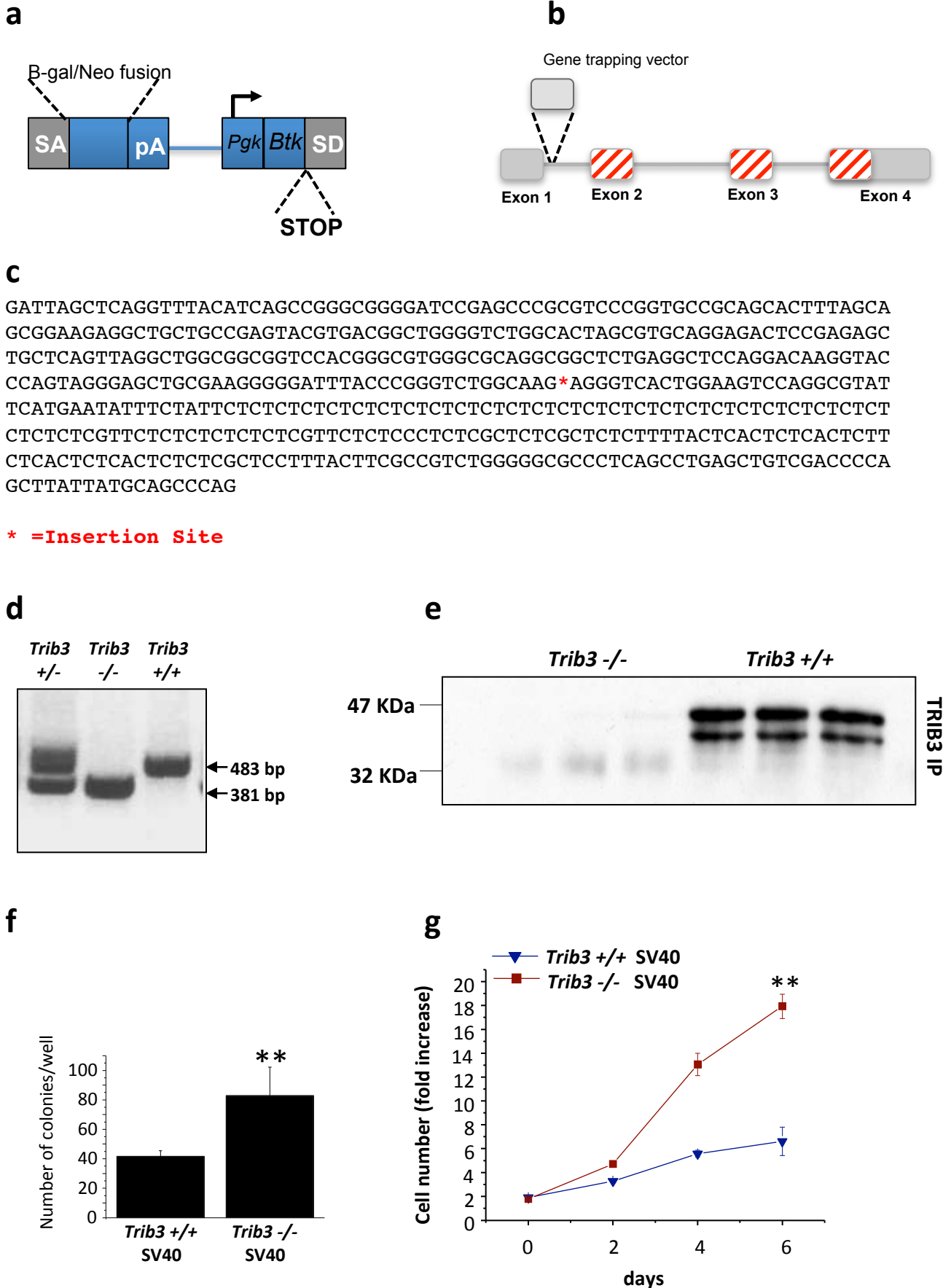


b



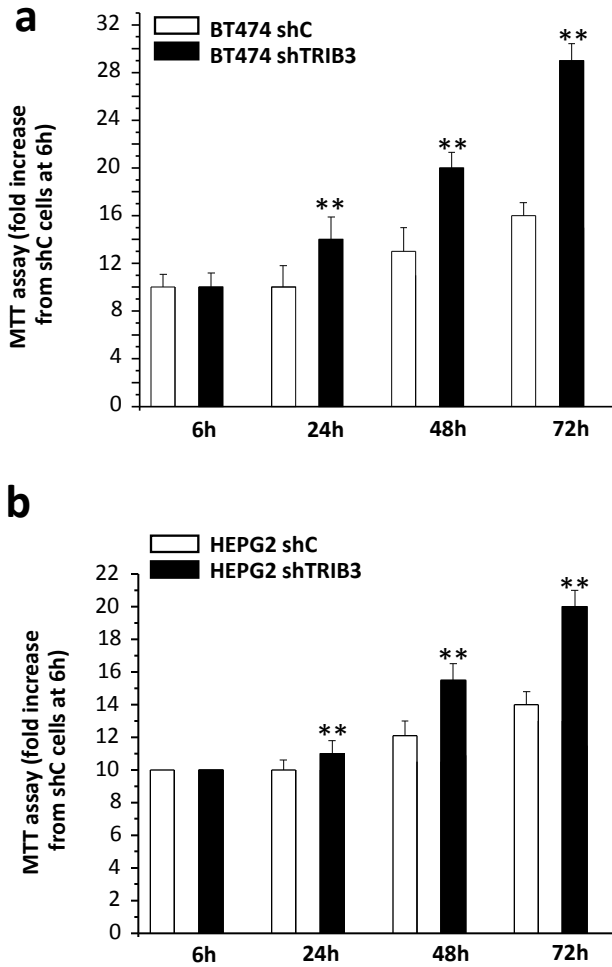






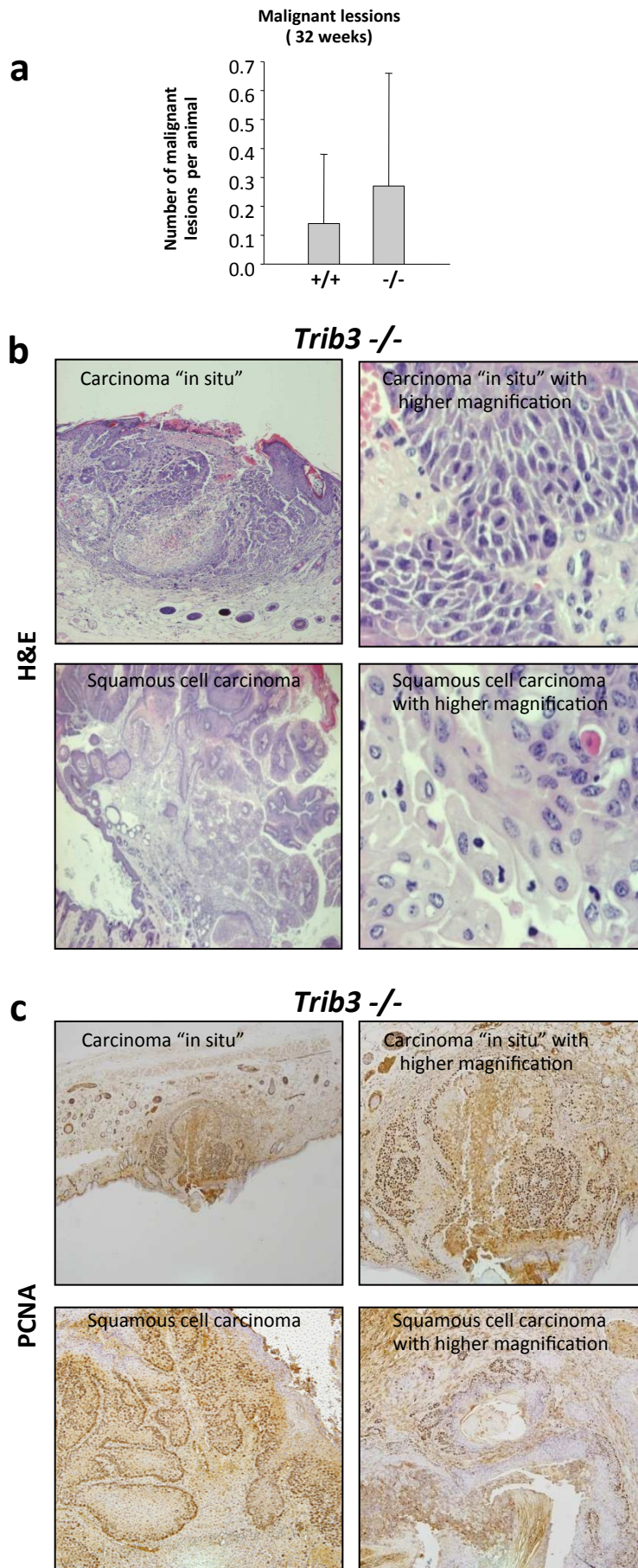
Supplementary Figure S1. Genetic inhibition of TRIB3 facilitates oncogene transformation and enhances the tumorigenicity of transformed embryonic fibroblasts.

(a-e) Generation of *Trib3*^{-/-} mice using the gene-trap system. (a) The gene trap vector used to inactivate the *Trib3* allele included two expression cassettes. The first cassette encoded for a splice acceptor site (SA), followed by a fusion protein of beta-galactosidase and neomycin, thereby disrupting transcription of the targeted mRNA. The second cassette encoded for a “diagnostic marker”, followed by a splice donor site and was used to determine the site of insertion for the targeting vector by 3' RACE. (b) Schematic showing the *Trib3* allele, which was targeted in the first intron using the gene-trap vector. (c) The sequence includes 250 nucleotides on either side of the insertion site, denoted by an asterisk (data kindly provided by Lexicon Pharmaceuticals). (d) PCR amplification (performed on genomic DNA obtained from *Trib3*^{+/+}, *Trib3*^{+/-} and *Trib3*^{-/-} mice) of the region where the gene trap vector is inserted (Forward primer hybridizes on *Trib3* exon-1 and reverse primers hybridize on intron 1-2 of the wild type allele and on the 5' region of the gene-trap vector, respectively). (e) Insertion of the gene trap vector prevents the expression of the TRIB3 protein. The panel shows TRIB3 protein levels as determined by immunoprecipitation and subsequent Western blot analysis in lysates obtained from cells derived from *Trib3*^{+/+} and *Trib3*^{-/-} animals. (f) Effect of the expression of SV-40 T-large antigen on the ability of *Trib3*^{+/+} and *Trib3*^{-/-} MEFs to form colonies in soft agar (cells were transduced with a retroviral vector encoding SV-40 T-large antigen). Data correspond to the number of colonies formed per dish in each experimental condition (mean ± SD; n = 3; ***P* < 0.01 relative to *Trib3*^{+/+} MEFs). (g) Effect of the expression of SV-40 T-large antigen on the number of *Trib3*^{+/+} and *Trib3*^{-/-} MEFs after several days in culture. Data correspond to the number of crystal-violet positive cells at each time point relative to the number of cells at day 0 for each experimental condition (mean ± SD; n = 3; ***P* < 0.01 relative to SV40-T large antigen-*Trib3*^{+/+} MEFs).



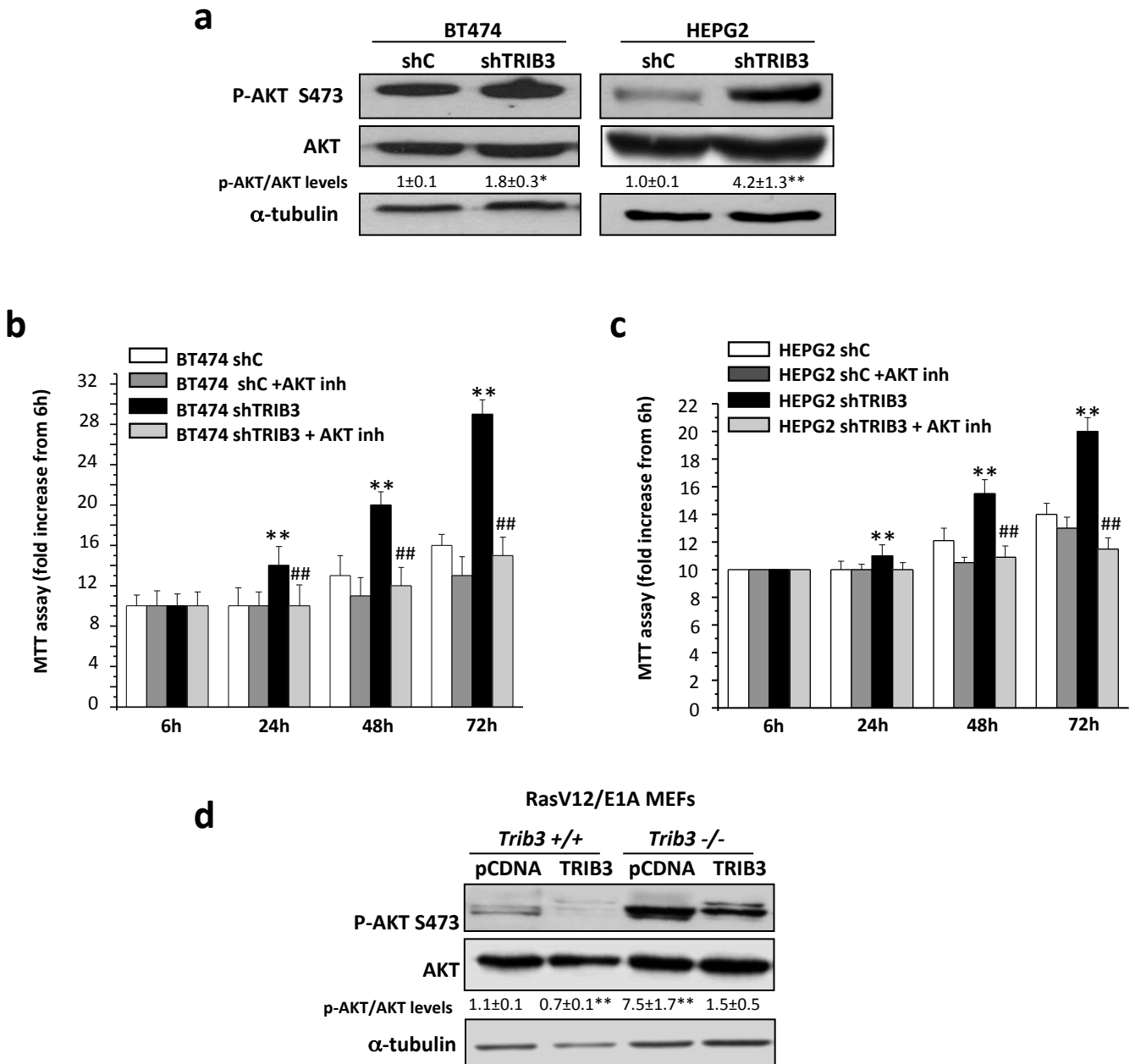
Supplementary Figure S2. Genetic inhibition of TRIB3 enhances the viability of cancer cell lines

Effect of TRIB3 stable knock-down on the number of shC and shTRIB3 BT474 (a) and HEPG2 (b) cells (as estimated by the MTT test) (mean \pm SD; n = 5; ** P < 0.01 from shC cells at each time point).



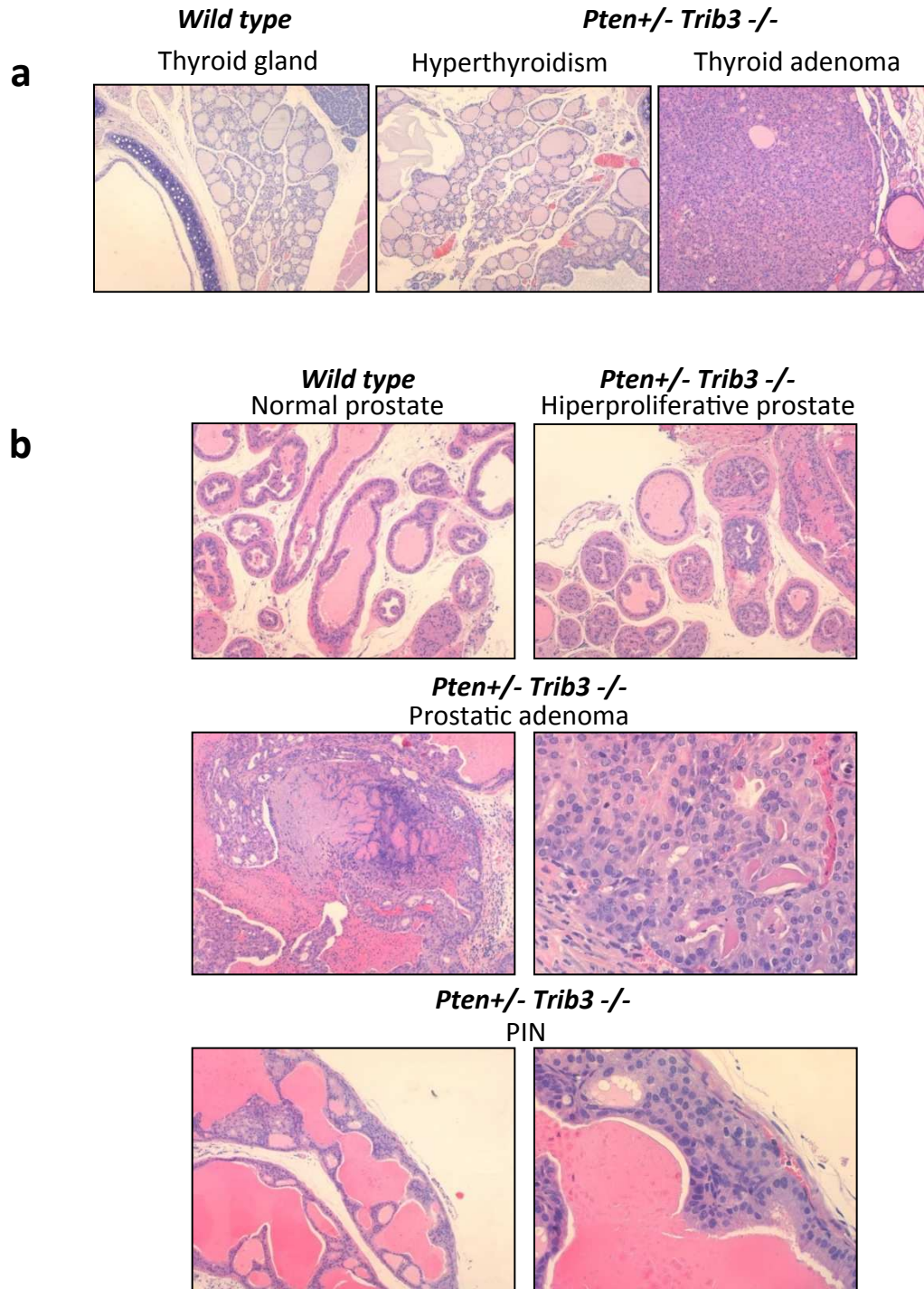
Supplementary Figure S3. Analysis of the effect of TRIB3 genetic deletion on the incidence of mouse skin carcinomas

(a) Effect of TRIB3 genetic inactivation on the incidence of skin carcinomas in *Trib3*^{-/-} and *Trib3*^{+/+} mice subjected to the two-stage skin carcinogenesis protocol (animals were sacrificed 20 or 32 weeks after the administration of the DMBA treatment and subsequently subjected to histopathological analyses). Data are expressed as the mean number of squamous cell carcinomas per animal \pm SEM) [7 *Trib3*^{+/+} and 9 *Trib3*^{-/-} mice sacrificed on week 32 were analyzed]. (b,c) Representative images of hematoxylin/eosin (b, left panels: 2x, right upper panel: 20x and right lower panel: 40x) and PCNA staining (c; left panels: 2x; right panels: 10x) of squamous carcinomas or in situ carcinomas observed in *Trib3*^{-/-} mice.



Supplementary Figure S4. Genetic inhibition of TRIB3 enhances the viability of cancer cell lines via AKT

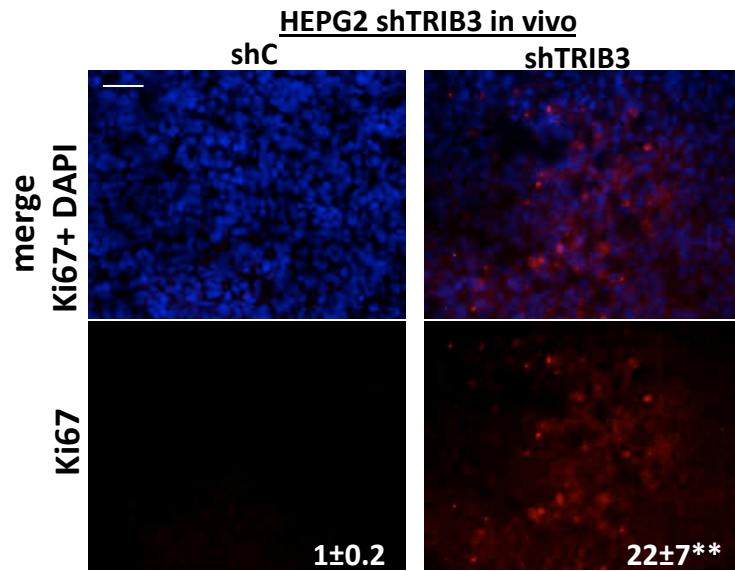
(a) Effect of TRIB3 stable knockdown on AKT phosphorylation of BT474 and HepG2 cells ($n = 3$; a representative Western blot for each cell line is shown). Values in the bottom of each Western blot correspond to the P-AKT/t-AKT ratio and are expressed as the mean fold change \pm SD relative to the corresponding shC cells; * $P < 0.05$ from shC cells). (b,c) Effect of TRIB3 stable knock-down and the AKT inhibitor X ($1 \mu\text{M}$; 24 h) on the number of BT474 (b) and HEPG2 (c) cells (as estimated by the MTT test) at the indicated time points (mean \pm SD; $n = 5$; ** $P < 0.01$ from shC vehicle-treated cells and ## $P < 0.01$ from shTRIB3 vehicle-treated cells). (d) Effect of TRIB3 re-expression on the phosphorylation of AKT on Ser 473 of RasV¹²/E1A-transformed *Trib3*^{+/+} or *Trib3*^{-/-} MEFs (a representative Western blot analysis is shown). Values in the bottom of the panels correspond to the P-AKT/t-KT ratio and are expressed as the mean fold change \pm s.d. relative to pCDNA-transfected, *Trib3*^{+/+} cells [$n=3$; ** $P < 0.01$ from pCDNA-transfected *Trib3*^{+/+} cells].



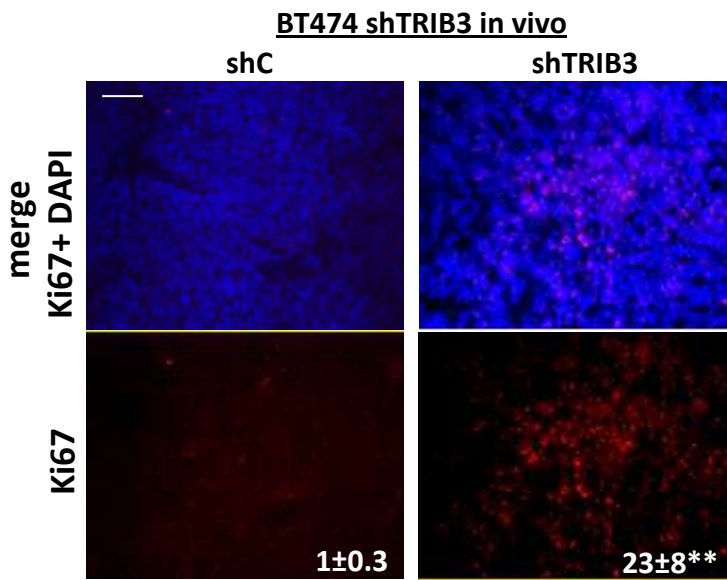
Supplementary Figure S5. Characterization of premalignant and malignant lesions in thyroid and prostate of *Pten*^{+/-} *Trib3*^{-/-} mice

(a,b) Representative microphotographs of the different lesions observed in the thyroid (a: 10x) and the prostate (b; upper panels: 10x, middle-lower left panels: 10x and middle-lower right panels: 40x) of *Pten*^{+/+} *Trib3*^{+/+} (WT) and *Pten*^{+/-} *Trib3*^{-/-} animals stained with hematoxylin/eosin.

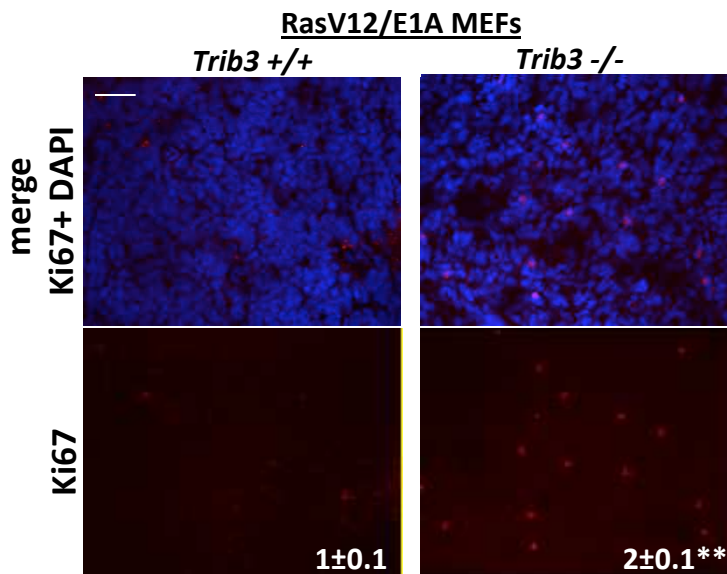
f



g



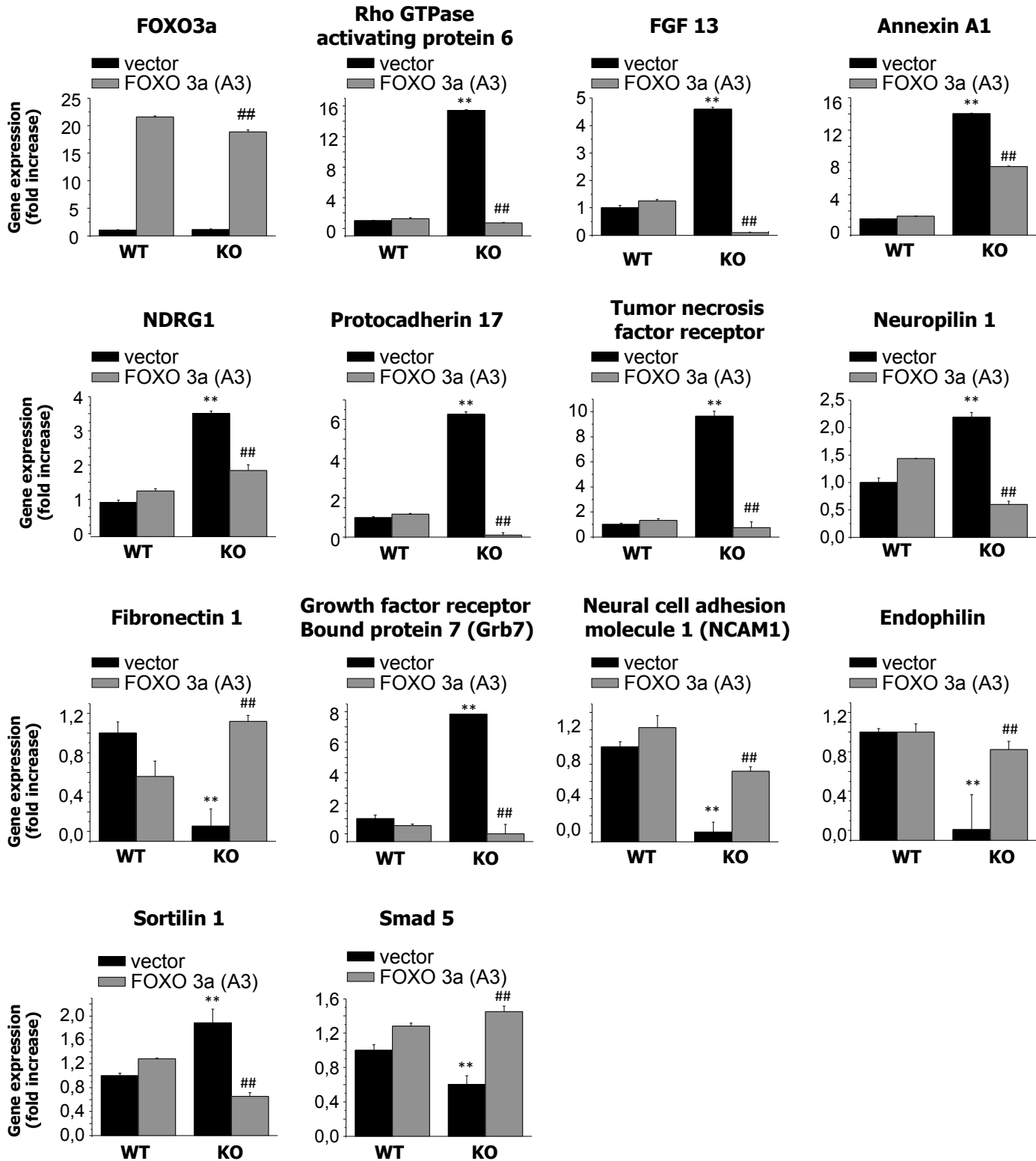
h

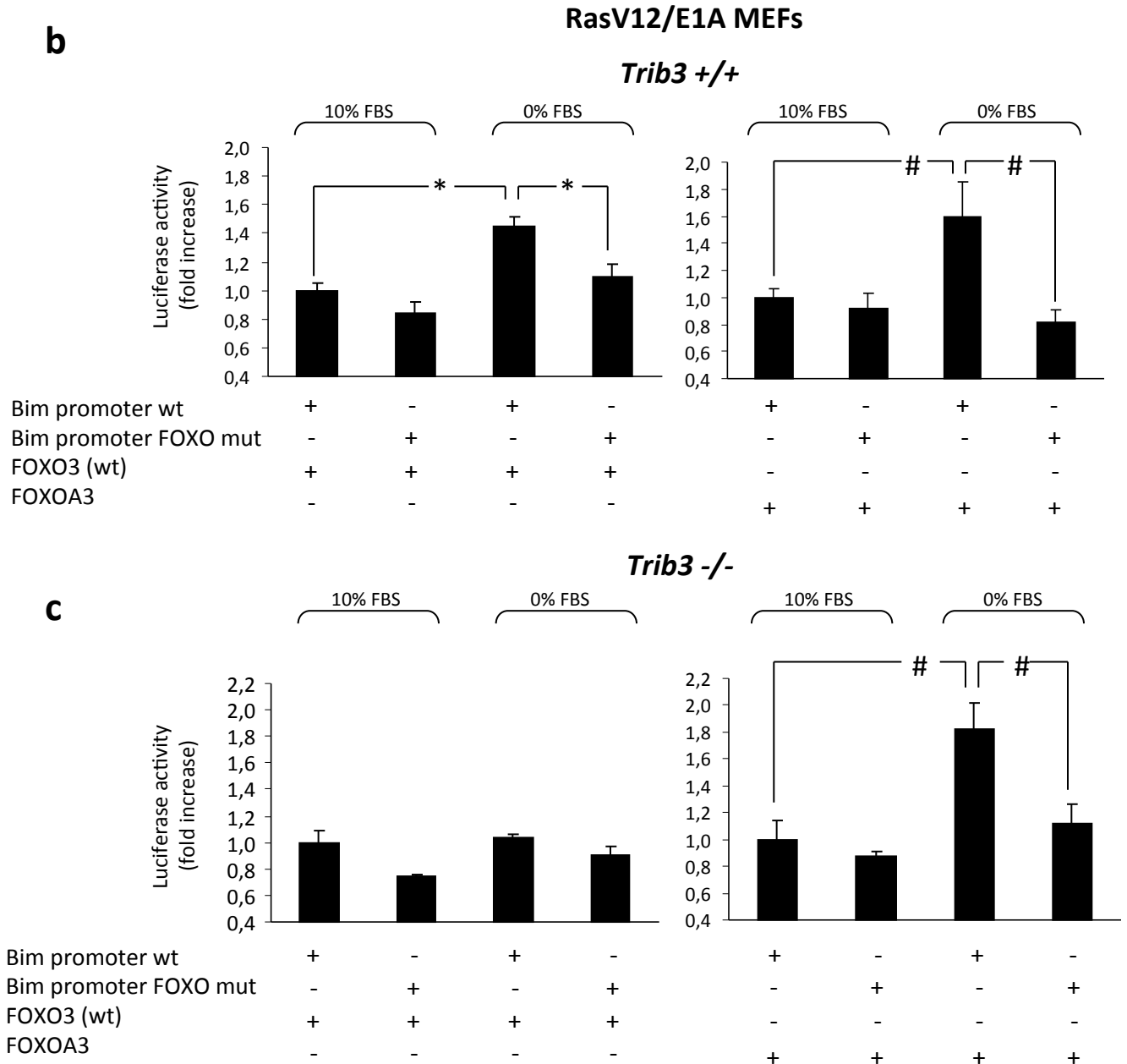


Supplementary Figure S6. Genetic inhibition of TRIB3 enhances the proliferation of cancer cell lines via AKT-dependent FOXO activation.

(a) Effect of TRIB3 genetic inactivation on the phosphorylation of BAD, PRAS40, GSK3 and S6 of Ras^{V12}/E1A-transformed MEFs (n=8; a representative experiment is shown). (b) Effect of TRIB3 stable knockdown on FOXO (upper panel) and S6 (lower panel) phosphorylation of BT474 and HepG2 cells (n=3; a representative Western blot for each cell line is shown). Values below the Western blots correspond to the densitometric analysis of the P-FOXO/t-FOXO levels (upper panel) or of the P-S6 levels with respect to the loading control and are expressed as the mean fold change \pm SD relative to the corresponding shC cells; ***P* < 0.01 from shC cells). (c) Effect of TRIB3 re-expression (upper panel), and RICTOR knock-down (lower panel) on the phosphorylation of BAD and PRAS40 of Ras^{V12}/E1A-transformed Trib3^{+/+} and Trib3^{-/-} MEFs (n=3; representative experiments are shown). RICTOR mRNA levels (as determined by real-time quantitative PCR) were reduced by 87 \pm 4 % in siRICTOR-transfected cells with respect to the levels of this mRNA in siC-transfected cells). (d) Effect of torin1 treatment (250nM, 18h) on the phosphorylation of FOXO (upper panel), BAD and PRAS 40 (lower panel) of Ras^{V12}/E1A-transformed Trib3^{+/+} and Trib3^{-/-} MEFs. Upper panel: values below the Western blot correspond to the densitometric analysis of the ratio P-FOXO/t-FOXO and are expressed as the mean fold change \pm s.d. relative to vehicle-treated (veh) Trib3^{+/+} cells. (n=3; ** *P* < 0.01 from Trib3^{+/+} cells) Lower panel: n=3; a representative experiment is shown. (e) Effect of serum withdrawal on the activity of the *Bim* promoter of Ras^{V12}/E1A-transformed Trib3^{+/+} and Trib3^{-/-} MEFs transfected with a vector encoding FOXO wild type and co-transfected with a luciferase reporter vector containing the sequence of the *Bim* promoter [wild type (wt) or mutated on the FOXO binding sites]. Data correspond to luciferase activity and are expressed as the mean fold change \pm SD relative to the corresponding *Bim* promoter (wt)-transfected cells incubated in the presence of serum (n = 4; **P* < 0.05 from serum-starved, *Bim* promoter (wt)- and FOXO3 (wt)-transfected cells). (f-h) Effect of TRIB3 stable knockdown or TRIB3 genetic inhibition on proliferation (as determined by Ki67 immunostaining) of tumor xenografts generated by subcutaneous injection of HepG2 cells (f) BT474 cells (g) and Ras^{V12}/E1A-transformed MEFs (h) in nude mice. For the immunostaining, values in the lower right corner of each panel correspond to the Ki67-positive cells normalized to the total number of nuclei in each section and are expressed as the mean fold change \pm SD relative to control tumors (18 sections for each of 3 dissected tumors for each condition were analyzed; ***P* < 0.01 from tumors generated with control cells).

a





Supplementary Figure S7. Loss of TRIB3 abrogates the FOXO-dependent activation of the *Bim* promoter in response to serum withdrawal

(a) Effect of TRIB3 genetic inactivation and stable expression of FOXOA3 on mRNA levels of different genes (as determined by real-time quantitative PCR) of RasV12/E1A-transformed *Trib3*^{-/-} MEFs (mean fold change relative to pBABE-*Trib3*^{+/+} cells ± SD; n=3; ***P* < 0.01 from pBABE *Trib3*^{+/+} cells ; ##*P* < 0.01 from pBABE-*Trib3*^{-/-} cells). (b,c) Effect of serum withdrawal on the activity of the *Bim* promoter of RasV12/E1A-transformed *Trib3*^{+/+} (b) and *Trib3*^{-/-} (c) MEFs transfected with a vector encoding FOXO wild type or FOXOA3 and co-transfected with a luciferase reporter vector containing the sequence of the *Bim* promoter [wild type (wt) or mutated on the FOXO binding sites]. Data correspond to luciferase activity and are expressed as the mean fold change ± SD relative to the corresponding *Bim* promoter (wt)-transfected cells incubated in the presence of serum (n = 4; **P* < 0.05 from serum-starved, *Bim* promoter (wt)- and FOXO3 (wt)-transfected cells and #*P* < 0.05 from serum-starved, *Bim* promoter (wt)- and FOXOA3-transfected cells).

Supplementary Table I. Cancer subtypes in which the chromosomal region where Trib3 gene is located has been found to be deleted

Data shown in the table were obtained from tumor scape data base and show that a portion of chromosome 20 containing the indicated number of genes, including Trib3, has been found to be deleted in tumors from the indicated origins (data were obtained from :

<http://www.broadinstitute.org/tumorscape/pages/portalHome.jsf?mode=publicHome>)

Cancer Subset	In Peak?	Nearest Peak	#Genes in Peak	Q-value	Frequency of Deletion		
					Overall	Focal	High-level
all_cancers	No	chr20:95685-297306	10	0,00217	0,1364	0,0364	0,0019
all_epithelial	Yes	chr20:95685-667854	17	0,165	0,163	0,0362	0,0026
Lung NSC	Yes	chr20:95685-2458642	37	0,191	0,2319	0,045	0,0027
Breast	Yes	chr20:95685-667854	17	0,231	0,1564	0,0453	0,0082
all_lung	Yes	chr20:95685-1818755	30	0,28	0,2287	0,0439	0,0026

Supplementary Table II. Decreased TRIB3 expression in human cancer samples

Cancer samples coming from 206 public experiments were investigated by the authors (Gene Expression Atlas - E-MTAB-62). The study compares the different cancer types to each other.

Tumor type	database entry	UP/ DOWN	T-Statistic	P-Value	publication
brain tumor	Gene Expression Atlas - E-MTAB-62	DOWN	-9.9	$< 1 \times 10^{-10}$	(2)
ovarian tumor	Gene Expression Atlas - E-MTAB-62	DOWN	-10	$< 1 \times 10^{-10}$	(2)
germ cell tumor	Gene Expression Atlas - E-MTAB-62	DOWN	-5.8	2.61×10^{-8}	(2)
uterine tumor	Gene Expression Atlas - E-MTAB-62	DOWN	-9.6	$< 1 \times 10^{-10}$	(2)
bladder cancer	Gene Expression Atlas - E-MTAB-62	DOWN	-3.3	2×10^{-3}	(2)
oral squamous cell carcinoma	Gene Expression Atlas - E-MTAB-62	DOWN	-3.5	1×10^{-3}	(2)
acute myeloid leukemia	Gene Expression Atlas - E-MTAB-62	DOWN	-12	$< 1 \times 10^{-10}$	(2)

Supplementary Table III. Selection of individual studies where decreased TRIB3 expression was detected

In these studies tumor samples were directly compared to normal tissue

Tumor type	database entry	UP/ DOWN	T-Statistic	P-Value	publication
breast tumor cells	GEO - GSE7515	DOWN	-4.9	1×10^{-3}	(3)
astrocytic tumor	Gene Expression Atlas - E-MEXP-567	DOWN	-3.4	4.7×10^{-2}	(4)
pituitary cancer	GEO - GSE26966	DOWN	-3.4	2.21×10^{-5}	(5)
ovarian serous carcinoma	GEO - GSE14001	DOWN	-4.4	1×10^{-3}	(6)
peripheral T-cell lymphoma	GEO- GSE19069	DOWN	-11	$< 1 \times 10^{-10}$	(7)

SUPPLEMENTARY METHODS

MEFs isolation

Mice (heterozygous for the gene of interest) were crossed and pregnant females were sacrificed on gestational day 13.5 to 14.5. Uterus (containing the embryos) was extracted and placed in a sterile 10 cm diameter dish; the amniotic sac was removed, and the embryos were dissected discarding the limbs, gut, liver and head (genomic DNA obtained from head were used for genotyping *TRIB3*). The remaining tissue was minced, incubated with trypsin at 37°C for 5 min, pipetted up and down to eliminate all clumps and incubated for 5 additional min at 37°C. Cell suspensions were transferred to 15 cm diameter plates with 25 ml of DMEM supplemented with 10% FBS and antibiotics. Medium was replaced 8-16 h after plating.

MEFs transformation using retroviral vectors

MEFs were transduced with supernatants enriched in retroviral particles, obtained from Phoenix Ecotropic cells. These cells (packaging cells) were plated in 10 cm diameter dishes with fresh medium (DMEM with 10% FBS). Cells reached 90% confluence on day of transfection. The day after, the Phoenix Ecotropic cells were transfected with a plasmid encoding a retroviral vector that includes the gene of interest using Lipofectamine 2000 (according to manufacturer's instructions; Invitrogen). After transfection, cells were incubated at 37°C / 5% CO₂ for 4-6 h and the medium was removed and replaced by fresh complete medium. In parallel, the day after transfection, MEFs (from wild-type and KO MEFs littermates) were plated in 10 cm diameter dishes with fresh complete medium (DMEM with 10% FBS), reaching 80 to 85% confluence on the day of infection. Forty-eight hours after transfection, the medium from Phoenix Ecotropic cells was collected, centrifuged to eliminate cell debris and filtered (0.45 µm).

Polybrene was added (5 µg/ml) to enhance the efficacy of retroviral transduction. Finally, the medium was removed from MEFs, the retroviral-enriched supernatant added and cells incubated at 37°C / 5% CO₂. The selection of transformed cells was performed with puromycin 3 or 4 days after transducing the cells with the retroviral particles. The concentration of antibiotics was increased gradually. Individual clones of puromycin-resistant cells were evident after several weeks of incubation in the selection medium. Individual clones were collected and amplified and the expected genotype was verified.

pBABE retroviral vectors were used to generate *Trib3*^{+/+} and *Trib3*^{-/-} MEFs stably expressing the following product genes: RasV12 /E1A (pBABE-RasV12 /E1A), RasV12 (pBABE-RasV12), SV40 – T large antigen (pBABE-SV40) or FOXO3aA3 (pBABE-FOXOA3). The vectors were kindly donated by Dr. Pier Paolo Pandolfi (Harvard Medical School, Boston, Massachusetts, US; pBABE-RasV12 /E1A, pBABE-RasV12 and pBABE-SV40) and by Dr. Clemens A. Schmitt (Max Delbrück Center, Berlin, Germany; pBABE-FOXO and pBABE FOXOA3).

Whole Genome Array process and data analyses

Whole genome expression characterization was conducted using MouseWG-6 v2.0 Expression BeadChips (Illumina Inc.). cRNA synthesis was obtained with TargetAmp™ Nano-g™ Biotin-aRNA Labeling Kit for the Illumina® System, Epicentre (Cat.Num. TAN07924) and subsequent amplification, labeling and hybridization were performed according to Whole-Genome Gene Expression Direct Hybridization Illumina Inc.'s protocol. Raw data were extracted with GenomeStudio analysis software (Illumina Inc.), in the form of GenomeStudio's Final Report (sample probe profile).

Sample intensity profiles showed no problems on standard quality controls (e.g. intensity distributions and sample correlation). Raw expression data were background-corrected, log₂-transformed and quantile-normalized using the lumi R package (8), available through the Bioconductor repository. Probes with a detection p-value lower than 0.01 in at least one sample were regarded as detected. For the detection of differentially expressed genes, a linear model was fitted to the probe data and empirical Bayes moderated t-statistics were calculated using the limma package (9) from Bioconductor.

Genetic knock-down by small interfering RNA

Mouse embryonic fibroblasts (MEFs) were transfected with siRNA duplexes using Dharma-FECT 1 Transfection reagent (Dharmacon, Lafayette, CO, US). Twenty-four hours after transfection, cells were trypsinized and seeded at a density of 5 000 cells/cm². Transfection efficiency was higher than 70% as monitored with a control fluorescent (red) siRNA (siGLO RISC-Free siRNA, Dharmacon). Human siRNAs to knock down RICTOR were purchased from Dharmacon as a SMARTpool. These reagents combine four SMARTselection designed siRNAs into a single pool, which guarantees an efficiency of silencing of at least 75%. The double stranded siRNA in all cases were designed and synthesized by Dharmacon. The non-targeted control (5'-UUCUCCGAACGUGUCACGU- 3'), was synthesized by Eurogentec (Liege, Belgium).

Infection with TRIB3 shRNA- human lentiviral particles

A pool of concentrated transduction-ready viral particles containing 3 shRNAs target-specific (or 3 shRNA non-targeted control) constructs (19-25 nt plus hairpin) (Santa

Cruz Biotechnology; Heidelberg, Germany) was used to stably knock-down the expression of TRIB3 in several tumor cell lines.

Briefly, cells were plated in 12-well dishes 24 h prior to viral infection. The day after, when the cells reached 50% confluence, medium was removed and replaced by complete medium with polybrene at a final concentration of 5 μ g/ml. Cells were subsequently infected with control- or TRIB3-selective shRNA lentiviral particles. The day after, the medium was removed and replaced by complete medium without polybrene. Finally, to select the clones stably expressing the shRNAs, the cells were incubated with puromycin 2 to 10 μ g/ml. Finally clones were selected and stable silencing confirmed by different approaches. At least 20 different selected clones were pooled for each of the cell lines generated. Following this procedure, we generated and tested the following cell lines: U87MG, HEPG2 or BT474 shC and shTRIB3 cells. Transformed/stably transfected MEFs correspond to a polyclonal mix of at least 20 different selected clones

Transfections of expression vectors

Transfections of expression vectors were performed with Lipofectamine 2000 according to the manufacturer's instructions (Invitrogen). See Supplemental Experimental procedures for a list of the plasmids used in this study. The plasmids pCDNA, pCDNA-HA-TRIB3 (kindly provided by Dr. Dario Alessi and Dr. Maria Deak; University of Dundee, Dundee, UK), pEBG-GFP, pEBG-PKB α , pEBG-pKB Δ PH, pEBG-PKB T308A, pEBG-PKB S473A, pEBG-PKB T308A/S473A, pEBG-PKB T308D, pEBG-PKB S473D, pEBG-PKB T308D/S473D (kindly provided by Dr. Jose Lizcano; Department of Biochemistry, Autonomia University, Barcelona, Spain), pCDNA-FOXO3a WT, pCDNA-FOXO3a (A3) (kindly provided by Dr. Pier Paolo Pandolfi)

were used throughout this work. For luciferase assays, the Firefly luciferase reporter plasmid containing 0.8 Kb of the *bim* promoter sequence along with a similar construct with mutated FOXO3 binding sites was kindly provided by Eric Lam (Imperial College London, London, UK). The pRL-TK (TK-Renilla luciferase) was a kind gift from B.M. Burgering (University Medical Center, Utrecht, The Netherlands).

Cell viability assays

Cell viability was determined by the MTT [(3-(4,5-Dimethylthiazol-2-yl)-2,5-diphenyltetrazolium bromide, a yellow tetrazole] test (Sigma Aldrich) following the manufacturer's instructions. Its absorbance at 570 nm, which is proportional to the amount of viable cells in the culture, was quantified by a spectrophotometer.

Luciferase assays

Cells were transfected with a luciferase reporter constructs containing different promoters along with a Renilla luciferase expression plasmid (pRL-TK) for normalization. Cells were lysed in passive lysis buffer and luciferase activity was analyzed using a luminometer and dual luciferase assay kit according to the manufacturer Promega (Medical Supply, Dublin, Ireland). Transfections were performed in triplicate dishes and Luciferase counts (RLUs) were normalized using TK Renilla luciferase co-transfection. Background luminescence was subtracted, and Luciferase activity was expressed as fold of the increase with respect to the control.

Western blot and immunoprecipitation

Cells were lysed on a buffer containing 50 mM Tris HCl, pH 7.5, 1 mM phenylmethylsulfonyl fluoride, 50 mM NaF, 5 mM sodium pyrophosphate, 1 mM sodium orthovanadate, 0.1% Triton X-100, 1 mg/ml leupeptin, 1mM EDTA, 1 mM

EGTA and 10 mM sodium β -glycerophosphate.

For immunoprecipitation experiments, cells were lysed on a buffer containing 40 mM Hepes pH 7.5, 120 mM NaCl, 1mM EDTA, 10 mM sodium pyrophosphate, 10 mM sodium glycerophosphate, 50 mM sodium fluoride, 0.5 mM sodium orthovanadate and 0.3% CHAPS. Briefly, lysate (1–4 mg) was pre-cleared by incubating with 5–20 μ l of Protein G–Sepharose coupled to pre-immune IgG. The lysate extracts were then incubated with 5–20 μ l of Protein G–Sepharose conjugated to 5–20 μ g of the antibody or pre-immune IgG (the antibody was previously covalently coupled to Protein G–Sepharose using dimethyl pimelimidate, from Sigma Aldrich). Immunoprecipitations were carried out overnight on a rotating wheel. The immunoprecipitates were washed 4 times with lysis buffer, followed by 2 washes with Hepes buffer (25 mM Hepes pH 7.5 and 50mM KCl). Then the immunoprecipitates were resuspended in 30 μ l of sample buffer (not containing 2 β -mercaptoethanol), filtered through a 0.22- μ m pore- size Spin-X filter and 2 β -mercaptoethanol was finally added to a concentration of 1% (v/v). Samples were subjected to electrophoresis and immunoblot analysis. Western blot analysis was performed following standard procedures. A list of the primary antibodies used is shown as a table at the end of the Supplementary methods section. Densitometric analysis was performed with Quantity One software (Bio-Rad; California, US).

Cytosolic and nuclear fractionation

Nuclear and cytosolic fractions were obtained from total cell lysates as described previously (10).

Reverse transcription-PCR

RNA was isolated by using Trizol Reagent (Invitrogen, following manufacturer's

instructions) and including a DNase digestion step with the RNasefree DNase kit (Qiagen; Maryland, US). cDNA was subsequently obtained using the first strand cDNA synthesis kit (Roche) or with the Transcriptor Reverse transcriptase (Roche). Human TRB3 sense (5'-GCCACTGCCTCCCGTCTTG-3') and antisense 5'-GCTGCCTTGCCCGAGTATGA-3') primers were used to determine the hTRIB3 levels in tumor samples derived from U87MG, BT474 and HEPG2 shC and shTRIB3 cells. Multi-species GAPDH sense (5'-GGGAAGCTCACTGGCATGGCCTTCC-3') and antisense (5'-CATGTGGGCCATGAGGTCCACCAC-3') primers were used to normalize as a control. PCR reactions were performed using the following parameters: 95°C for 5 min, 94°C for 30 s, 52°C for 30 s, and 72°C for 1 min, followed by a final extension step at 72°C for 5 min. The number of cycles was adjusted to allow detection in the linear range.

Real-time quantitative PCR

cDNA was obtained with Transcriptor (Roche). Real-time quantitative PCR assays were performed using the FastStart Master Mix with Rox (Roche) and probes were obtained from the Universal Probe Library Set (Roche). Primer sequences and Roche's probes corresponding to each pair of primers can be found in supplemental table 3. Amplifications were run in a 7900 HT-Fast Real-Time PCR System (Applied Biosystems; California, US). Each value was adjusted by using 18S RNA levels as reference.

Cell invasion assay

The cell invasion was monitored using cell culture matrigel invasion chambers (BD Biosciences, Bedford, MA). Briefly, cells were trypsinized, washed, resuspended in

DMEM 0.1% FBS and loaded into the insert (50 000 cells/chamber). DMEM supplemented with 10% FBS was placed in the plate well as a cell migration stimulus. Cells were allowed to migrate for 24 h at 37°C through an 8- μ m polyethylene terephthalate tracketched membrane included in the matrigel invasion chambers (BD Biosciences). Then, cells from the upper side of the membrane were removed. The remaining cells on the bottom side of the membrane were fixed with 4% paraformaldehyde (10 min at room temperature) and stained with DAPI (Invitrogen; 10 min, room temperature) before montage with Mowiol was performed. Fluorescence images were acquired using a Zeis Axioplan 2 Microscope.

Soft agar colony formation assay: anchorage independent growth

Briefly, sterilized 0.5% agar and 0.35% agar in DMEM supplemented with 10% FBS were melted in a microwave and cooled to 37°C in a water-bath. 1.5 ml of 0.5% agar complete medium was added to each well in a 6-well plate and set aside for several minutes to allow agar solidification. Cells were then trypsinized, washed and resuspended in complete medium at a final concentration of 200 000 cells/ml. One hundred μ l of this preparation were mixed with 6 ml of 0.35% agar complete medium and 1.5 ml (5 000 cells) of these mixtures were carefully added to each well (over the base layer) and incubated at 37°C 5% CO₂ for 7-28 days. The resulting colonies were morphologically assessed and quantified after staining with crystal violet (0.05% in 25% methanol).

***In vivo* generation of tumor xenografts**

Tumors were induced by subcutaneous injection in nude mice (Harlan Interfauna Iberica, Barcelona, Spain) of 4 x10⁶ cells (RasV¹²/E1A-Trib3^{+/+} and Trib3^{-/-} MEFs, empty vector- or FOXOA3-RasV¹²/E1A-transformed Trib3^{+/+} and Trib3^{-/-} MEFs; shC-

or shTRIB3-HEPG2, BT474 and U87MG cells) in PBS supplemented with 0.1% glucose. Tumors were routinely measured with external caliper, and volume was calculated as $(4\pi/3) \times (\text{width}/2)^2 \times (\text{length}/2)$.

Confocal microscopy and Immunofluorescence of cells and tumor samples

Cell cultures grown on 12 mm-coverslips were washed in PBS, fixed with 4% paraformaldehyde (20 min at room temperature), permeabilized with 0.5% Triton X-100 (5 min at room temperature), incubated with the corresponding primary antibodies (for a detailed list of the antibodies used in immunofluorescence experiments, see table at the end of the Supplementary Methods section), washed and incubated with Alexa-488 or Alexa-594-conjugated secondary antibodies (Invitrogen; Carlsbad, California, US) in the dark at room temperature for 1 h. Cell nuclei were stained with Hoechst 33342 (Invitrogen). Finally, coverslips were mounted in ProLong Gold antifade reagent (Invitrogen) and visualized in a Leica TCS SP2 confocal microscope.

Samples from tumor xenografts were dissected, Tissue-Tek (Sakura; South Carolina, US) embedded and, before the staining procedures were performed, fixed in acetone for 10 min at room temperature and frozen. After fixation, sections (5 μm) were permeabilized and blocked to avoid non-specific binding with 10% goat antiserum and 0,25% Triton X-100 in PBS for 45 min and subsequently incubated with the primary antibodies shown in Supplemental table 2. Then, samples were washed, incubated with the corresponding Alexa-488 or Alexa-594-conjugated secondary antibodies (Invitrogen; 90 min, room temperature) and nuclei were stained with DAPI (Invitrogen; 10 min, room temperature) before montage with Mowiol mounting medium (Merck, Darmstadt, Germany) was performed. Fluorescence images were acquired using Metamorph-Offline 6.2 software (Universal Imaging) and Zeiss Axioplan 2

Microscope.

Immunohistochemistry

Paraffin-embedded sections from tumors were deparaffinized and rehydrated using standard protocols and subjected to heat-induced antigen retrieval in citrate buffer. Endogenous peroxidase blockade and unspecific binding reduction were achieved by successive incubation with 3% H₂O₂ and 5% goat serum (Abcam) supplemented with 3% BSA and 1% Triton X-100 (Sigma), respectively. Samples were then incubated with an anti-pAKTSer473 antibody (1/100), an anti-pFOXO antibody (1/100) or an anti-PCNA antibody (1/400) and further processed with appropriate secondary antibodies following the LSAB2 horseradish peroxidase kit's instructions (Dako cytometry, Carpinteria, CA). Hematoxylin were used for nuclei staining. Images were acquired with Cell^A software (Olympus, Münster, Germany)

List of antibodies used in Western blot analyses

Antigen	Host	Company
TRB3 Nt	rabbit	Abcam, Cambridge, UK
Phospho-Akt (Ser473)	rabbit	Cell Signaling
Phospho-Akt (Thr308)	rabbit	Cell Signaling
Total Akt	sheep	Kindly donated by Dr. Dario Alessi
Phospho-FoxO1 (Thr24)/FoxO3a (Thr32)	rabbit	Cell Signaling
Total FoxO3a	rabbit	Cell Signaling
Phospho-Bad (Ser136)	mouse	Cell Signaling
Total Bad	rabbit	Cell Signaling
phospho-PRAS40 (Thr246)	sheep	Kindly donated by Dr. Dario Alessi
Total PRAS40	sheep	Kindly donated by Dr. Dario Alessi
Phospho-GSK3 α (Ser 9)	rabbit	Cell Signaling
Total GSK3 α	rabbit	Cell Signaling
phospho-S6 ribosomal protein (Ser 235/236)	rabbit	Cell Signaling
Total S6 ribosomal protein	mouse	Cell Signaling
Cleaved caspase 3 (Asp175)	rabbit	Cell Signaling
HA	rat	Santa Cruz Technology
Lamin A/C	rabbit	Cell Signaling
IKB α	rabbit	Santa Cruz Biotechnology
β actin	mouse	Sigma Aldrich
α tubulin	mouse	Sigma Aldrich

List of antibodies used in immunofluorescence or immunohistochemistry analyses

Antigen	Host	Company
Cleaved caspase 3 (Asp175)	rabbit	Cell Signaling
Ki67	rabbit	Neomarkers
Phospho-Akt (Ser473)	rabbit	Cell Signaling
Phospho-FoxO1 (Thr24)/FoxO3a (Thr32)	rabbit	Cell Signaling
Total FoxO3a	rabbit	Cell Signaling
PCNA	mouse	Abcam

List of primers used in quantitative PCR analyses

Gene	Specie	Primers	Probe
TRB3	mouse	CGCTTTGTCTTCAGCAACTG TCATCACGCAGGCATCTTC	67
RICTOR	mouse	AGTGAATCTGTGCCATCGAGT AAGGAAAAATGTGCTAGTAGAGCTG	88
FOXO3a	mouse	CTTCAAGGATAAGGGCGACA GACAGATTGTGGCGAATTGA	11
Rho GTPase- activating protein	mouse	TGGCTCCAGCAGAGGAAG CATGCTGTTCCAGGTGAAGTC	75
Fibroblast Growth Factor 13	mouse	AGGCAGATGGAACCATTGAT CCCACAGGGATGAGGTTAAA	56
Annexin A1	mouse	GTGAACGTCTTCACCACAATTC GTACTTTCCGTAATTCTGAAACACTCT	18
NDRG1	mouse	TTCATCAGCGCCTACAACAG AGTGTGGGTTCCAGGCATT	80
Protocadherin 17	mouse	GCCACTCGGATGTCCATAAT GGTCCTTAAACGTGGAGCTA	27
Tumor necrosis factor receptor	mouse	GGAAAGTATGTCCATTCTAAGAACAA AGTCACTCACCAAGTAGGTTCTT	84
Neuropilin 1	mouse	CCACACACAGTGGGCTTG GGTCCAGCTGTAGGTGCTTC	26
Fibronectin 1	mouse	CGGAGAGAGTGCCCCTACTA CGATATTGGTGAATCGCAGA	52
Growth factor receptor Bound protein 7 (Grb7)	mouse	GTCCGGCTCCTTCTGTTG GGGAGCTGCTGAGATGAGTC	1
Neural cell adhesion molecule 1 (NCAM1)	mouse	AGGGCAAGGCTGCTTTCT CCCCATCATGGTTTGGAGT	69
Endophilin	mouse	CCGCCCTGAAGGAGATAAC CTCAATTCCTGTTTCAGATTTTGTC	6
Sortilin 1	mouse	CGGATATCACGACGACTCAG GAGCCTCAGGGAGTGTAGGA	17
Smad 5	mouse	GCAGTAACATGATTCCTCAGACC GCGACAGGCTGAACATCTC	107

BIM	mouse	GGAGACGAGTTCAACGAACTT AACAGTTGTAAGATAACCATTTGAGG	41
18S RNA	multi- species	GCTCTAGAATTACCACAGTTATCCAA AAATCAGTTATGGTTCCTTTGGTC	55

Supplementary references

1. Santo EE, Stroeken P, Sluis PV, Koster J, Versteeg R, Westerhout EM. FOXO3a is a major target of inactivation by PI3K/AKT signaling in aggressive neuroblastoma. *Cancer Res* 2013 Apr 1; **73** (7): 2189-2198.
2. Lukk M, Kapushesky M, Nikkila J, Parkinson H, Goncalves A, Huber W, *et al.* A global map of human gene expression. *Nat Biotechnol* 2010 Apr; **28** (4): 322-324.
3. Creighton CJ, Li X, Landis M, Dixon JM, Neumeister VM, Sjolund A, *et al.* Residual breast cancers after conventional therapy display mesenchymal as well as tumor-initiating features. *Proc Natl Acad Sci U S A* 2009 Aug 18; **106** (33): 13820-13825.
4. Margareto J, Leis O, Larrarte E, Idoate MA, Carrasco A, Lafuente JV. Gene expression profiling of human gliomas reveals differences between GBM and LGA related to energy metabolism and notch signaling pathways. *J Mol Neurosci* 2007; **32** (1): 53-63.
5. Michaelis KA, Knox AJ, Xu M, Kiseljak-Vassiliades K, Edwards MG, Geraci M, *et al.* Identification of growth arrest and DNA-damage-inducible gene beta (GADD45beta) as a novel tumor suppressor in pituitary gonadotrope tumors. *Endocrinology* 2011 Oct; **152** (10): 3603-3613.
6. Tung CS, Mok SC, Tsang YT, Zu Z, Song H, Liu J, *et al.* PAX2 expression in low malignant potential ovarian tumors and low-grade ovarian serous carcinomas. *Mod Pathol* 2009 Sep; **22** (9): 1243-1250.
7. Iqbal J, Weisenburger DD, Greiner TC, Vose JM, McKeithan T, Kucuk C, *et al.* Molecular signatures to improve diagnosis in peripheral T-cell lymphoma and prognostication in angioimmunoblastic T-cell lymphoma. *Blood* 2009 Feb 4; **115** (5): 1026-1036.
8. Du P, Kibbe WA, Lin SM. lumi: a pipeline for processing Illumina microarray. *Bioinformatics* 2008 Jul 1; **24** (13): 1547-1548.
9. Smyth GK. Limma: linear models for microarray data. In: R. Gentleman VC, S. Dudoit, R. Irizarry, W. Huber (ed). *Bioinformatics and Computational Biology Solutions using R and Bioconductor*. Springer: New York, 2005, pp 397-420.
10. Essafi A, Gomes AR, Pomeranz KM, Zwolinska AK, Varshochi R, McGovern UB, *et al.* Studying the subcellular localization and DNA-binding activity of FoxO transcription factors, downstream effectors of PI3K/Akt. *Methods Mol Biol* 2009; **462**: 201-211.